Discovery and characterization of ORM-11372, a unique and positively inotropic sodium-calcium exchanger/inhibitor

Short running title: Discovery and characterization of the NCX inhibitor ORM-11372

Leena Otsomaa[1], Jouko Levijoki[1], Gerd Wohlfahrt[1], Hugh Chapman[1], Ari-Pekka Koivisto[1], Kaisa Syrjänen[1] Tuula Koskelainen[1], Saara-Elisa Peltokorpi[1], Piet Finckenberg[2], Aira Heikkilä, Najah Abi-Gerges[3], Andre Ghetti[3], Paul E. Miller[3], Guy Page[3], Eero Mervaala[2], Norbert Nagy[4,5], Zsófia Kohajda[4], Norbert Jost[4,5], László Virág[5], András Varró[4,5], Julius Gy. Papp[4,5]

[1]Orion Pharma R&D, Orionintie 1, P.O.Box 65, 02101 Espoo, Finland
[2]Department of Pharmacology, Faculty of Medicine, Helsinki, Finland
[3]ANABIOS Corporation, 3030 Bunker Hill Street #312, San Diego, CA 92109
[4]MTA-SZTE Research Group of Cardiovascular Pharmacology, Hungarian Academy of Sciences, Szeged
[5]Department of Pharmacology and Pharmacotherapy, Interdisciplinary Excellence Centre, Faculty of Medicine, University of Szeged, Szeged, Hungary

Word count: 3956

Abstract

Background and purpose

The lack of selective sodium-calcium exchanger (NCX) inhibitors has hampered the exploration of physiological and pathophysiological roles of cardiac NCX 1.1. We aimed to discover more potent and selective drug like NCX 1.1. inhibitor.

Experimental approach

A flavan series-based pharmacophore model was constructed. Virtual screening helped us identify a novel scaffold for NCX inhibition. A distinctively different NCX 1.1 inhibitor, ORM-11372, was discovered after lead optimization. Its potency against human and rat NCX 1.1 and selectivity against other ion channels was assessed. The cardiovascular effects of ORM-11372 were studied in normal and infarcted rats, and rabbits. Human cardiac safety was studied *ex-vivo* using human ventricular *trabeculae*.

Key results

ORM-11372 inhibited human NCX 1.1 reverse and forward currents; IC_{50} values were 5 and 6 nM, respectively. ORM-11372 inhibited human cardiac sodium 1.5 (I_{Na}) and hERG K_V11.1 currents (I_{hERG}) in a concentration-dependent manner; IC_{50} values were 23.2 and 10.0 μM. ORM-11372 caused no changes in action potential duration; short term variability and triangulation were observed for concentrations of upto 10 μM.

ORM-11372 induced positive inotropic effects in 18 ± 6% and 35 ± 8% anesthetized rats with myocardial infarctions and rabbits, respectively; no other haemodynamic effects were observed, except improved relaxation at the lowest dose.

This article has been accepted for publication and undergone full peer review but has not been through the copyediting, typesetting, pagination and proofreading process which may lead to differences between this version and the Version of Record. Please cite this article as doi: 10.1111/bph.15257

Conclusion and implications

ORM-11372, a unique, novel, and potent inhibitor of human and rat NCX 1.1, is a positive inotropic compound. NCX inhibition can induce clinically relevant improvements in left ventricular contractions without affecting relaxation, heart rate, or blood pressure, without pro-arrhythmic risk.

Keywords:

Sodium-calcium exchanger; NCX; ORM-11372; positive inotropic effect; cardiac safety

Abbreviations

A_{max}	Maximum amplitude of action potential
AP	Action potential
APD_{90}	Action potential duration 90%
ARRIVE	Animal research: reporting in vivo experiments
Ca_v	Voltage dependent Ca^{2+} channel
CHO-K1	Chinese Hamster Ovary cells, subtype
cLogP	Calculated logarithm of partition coefficient
cLogS	Calculated logarithm of solubility
CM	Cardiomyocyte
ECC	Exitation-contraction coupling
FCCP	Carbonyl cyanide 4-(trifluoromethoxyl)
Fluo-4	Ca^{2+} dye
[^{3}H]NE	Tritium labelled norepinephrine
HAM F-12	Ham's Nutrient Mixture F12
HIPAA	Health Insurance Portability and Accountability Act
HR	Heart rate
hSCN5	Human sodium voltage-gated channel subunit 5
I_{CAL}	L-type Ca^{2+} channel current
I_{hERG}	Human ether-á-go-go-related gene-encoded voltage dependent potassium channel current
IMR-32	Human neuroblastoma cell line
I_{Na}	Human cardiac sodium 1.5 current
I_{NCX}	Na^+/Ca^{2+} exchanger current
hiPSC	Human induced pluripotent stem cell
IRB	Institutional Review Board
KATP	ATP dependent potassium channel
KCNH2	Potassium Voltage-Gated Channel, Subfamily H (Eag-related), Member 2
K_v	Voltage dependent potassium channel
K_v11.1	Alpha subunit of a potassium ion channel
LQT	Long QT time
LVP	Left ventricular pressure
LV+dP/dtmax	Left ventricular inotropic effect
LV-dP/dtmin	Left ventricular relaxation
m-	Meta-position
MEM	Minimum Essential Medium
MI	Myocardial infarction
mOsm	Milliosmoles
MRSA	Methicillin-resistant *Staphylococcocus aureus*

Na_2ATP	Adenosine 5′-triphosphate disodium salt hydrate
$NaBH_4$	Sodium borohydride
$Na_v1.5$	Voltage-gated sodium channel, alpha subunit 5
NC3Rs	National centre for replacement, refinement, reduction of animals in research
NCX	Sodium-calcium exchanger
NCX_{IF}	Intrinsic factor inhibiting NCX
NIH	National Institute of Health
PMCA	Plasma membrane Ca^{2+} ATPase
p-	Para-position
RMP	Resting Membrane Potential
rpm	rounds per minute
SAR	Structure Activity Relationship
SCN5A	Voltage-gated sodium channel alpha subunit 5 (i.e.Nav1.5)
Sf9	Insect cell *Spodoptera frugiperda*
SKCa	Small conductance calcium dependent potassium channel
SLC8	Solute carrier transporter gene family
SP	Systemic blood pressure
STV	Short term variability analysis of action potential duration
TEACl	Tetraethylammonium Chloride
TNM-FH	Insect cell culture medium
XIP	Exchanger inhibiting peptide

Summary:

What is already known

- NCX plays a pathological role in heart failure, cardiac ischemia, and arrhythmia.
- Known NCX modulators are unselective small molecules or peptides.

What this study adds

- The newly-discovered NCX inhibitor was the most potent and selective.
- Positive inotropic effect in *in vivo* rabbits and no pro-arrhytmic risk in human cardiac tissue.

Clinical significance

- Positive inotropic effect without effects on other haemodynamic parameters.

Introduction

Sodium-calcium exchanger (NCX) has dynamic role in exitation-contraction coupling (ECC) in cardiomyocytes. The driving force of NCX depends on sodium and calcium concentrations across cell membrane cell as well as membrane potential. NCX operates dominantly in the forward mode (Ca^{2+} extrusion and inducing depolarizating current) during systole in all species. Therefore, selective NCX inhibitors have only minor effect on peak $[Ca^{2+}]_i$ in mice and dogs (Kohajda et al., 2016; Kormos et al., 2014; Oravecz et al., 2018). In addition, both mechanical relaxation and $[Ca^{2+}]_i$ decay remained unchanged (Kormos et al., 2014). Selective NCX inhibitors either slightly shorten action potential duration or have no effect in normal oxygen and ionic conditions. Overall it seems that selective NCX inhibition has minimal effect on intracellular Ca^{2+} or APD under normal conditions.

In heart failure, the intracellular Ca^{2+} concentration balance is changed, and the role of NCX becomes even more important (Bers et al., 2006). In addition, NCX and intracellular Ca^{2+} regulate each other and affect cardiac remodeling, as described in a very recent study (Primessnig et al., 2019). ORM-11035, a selective NCX inhibitor, attenuated cardiac hypertrophic remodeling and prevented cardiac dysfunction in rats exhibiting heart failure. NCX also reportedly controls the heart rate through its effects on the sinus and atrioventricular nodes (Kaese et al., 2017). In sinus node, funny current (I_f) and NCX current (I_{NCX}) together establish a strong depolarization capacity providing important safety factor for stable pacemaking (Kohajda et al., 2019). NCX also plays a role in blood pressure control in normotensive and hypertensive individuals (Zhang, 2013).

The SLC8 gene family encodes several Na^+/Ca^{2+} exchanger subtypes. SLC8A1 gene overexpression and NCX1.1 protein upregulation is linked to many pathological conditions that lead to reduced contractility and arrhythmias (Khananshvili, 2013). NCX is organized into ten transmembrane segments and is localized in the sarcolemmal membrane (Jost et al., 2013; Shattock et al., 2015). Two Ca^{2+} binding domains are known currently. Their activation is regulated by Ca^{2+} binding at these sites, whereas Na^+ binding leads to NCX inactivation (Hilgemann et al., 1992).

Several potent NCX inhibitors have been reported (Table S1). In 1996, KB-R7943 was the first NCX inhibitor to be discovered. SN-6 (Iwamoto et al., 2004) and SEA0400 (Matsuda et al., 2001) were reported to be more selective NCX inhibitors than KB-R7943. YM-244769 (Iwamoto et al., 2006), which was discovered in 2006, was reported to be a novel NCX inhibitor with higher selectivity. ORM-10103 (Koskelainen et al., 2003) was discovered in 2013, followed by ORM-10962 (Otsomaa et al., 2004) and GYKB-6635 (Geramipour et al., 2016) in 2016; they were highly selective NCX inhibitors (Jost et al., 2013; Kohajda et al., 2016). Despite their higher selectivity, their poor solubility as positive inotropic tool compounds in *in vivo* experiments (solubility of SEA0400 is less than 10 µg/ml into pH 7.4 phosphate buffer i.e. solubility class insoluble) prevented their use. ORM-10962 is an exception from previously reported selective NCX inhibitors, as it exhibits reasonable solubility in *in vivo* studies.

Here, we describe the discovery of a new type of positive inotropic compound, ORM-11372, exhibiting high NCX1.1 selectivity and pharmacological profiling *in vitro*, *in vivo,* and *ex-vivo* in human ventricular *trabeculae*. ORM-11372 was developed for acute short-term use with fast clearance.

Materials and Methods

Discovery of a novel chemical series

A novel and unique chemical series was discovered using ligand-based pharmacophores for virtual screening with Catalyst (Accelrys) (Figure 1A). Pharmacophore features used for virtual screening were derived from previously discovered NCX1 inhibitor flavan structures, such as ORM-10103 (Koskelainen et al., 2003) and ORM-10962 (Otsomaa et al., 2004). Based on the results of virtual screening, a proposed library with 636 commercially available compounds was selected for testing in the fluorescence-based assay, at concentrations of 10 µM. The original hit ORM-120407 inhibited NCX1.1 by 87% and had an IC_{50} value of ~200 nM. It inhibited hERG and L-type Ca^{2+} channels, with IC_{50} values of 2.1 µM and 3.1 µM, respectively. These results indicated that the scaffold exhibited

optimization potential. The SAR of ORM-120407 was explored; thus, ORM-11372 (Table 1 and Figure 2) was discovered during medicinal chemistry optimization.

An analysis of 250 previously discovered NCX inhibitor compounds by Orion (Koskelainen et al., 2003; Otsomaa et al., 2004) resulted in a 5-feature pharmacophore, which was used for the virtual screening of Chambridge and Spcs compound libraries. In-silico hits were further filtered based on predicted activity, clogS, clogP, and diversity. The substructure features were optimized in parallel processes and beneficial structural features were merged, in order to identify the potential overall synergistic effects for NCX1.1 inhibition. Representative samples of 135 synthesized derivatives are presented in Figure 2.

The hydrogen bond donor property of aniline in the original hit molecule ORM-120407 was proven to be important for NCX1.1 activity in the scaffold. The addition of polar substituents was not tolerated in the A ring, but halogen substitution on the *p*- and *m*- positions were tolerated, and resulted in improved NCX1 inhibition. However, neither position was favoured over the other, and none showed synergistic or additive effects. Their selectivity towards the hERG channel was found to be its differentiating property.

SAR tolerated 5-membered B-ring systems better than 6-membered systems. Ring heteroatoms *i.e.* oxygen or nitrogen molecules at position one (of furan) in combination with a 1-, 5- substitution was proven to be critical for binding, *i.e.* a carbon at position 1 abolished activity. This finding indicates that the presence of a hydrogen bond acceptor at that position is important. B-ring optimization provided three potential ring systems that were tolerated; furans, oxazoles, and thiazoles. Two latter systems tolerated 4,2- and 2,4- substitutions, while the three heteroatoms in the B-ring reduced NCX1 inhibition activity. Though ORM-120407 showed good inhibitory activity towards NCX1, its selectivity towards hERG (2.1 μM) and L-type calcium (3.1 μM) channels needed to be improved. ORM-120407 also had poor solubility (<10 μg/ml). ORM-11298 exhibited better inhibitory activity towards NCX1 and good selectivity towards hERG channels. The oxazole series also exhibited good selectivity towards L-type calcium channels such as ORM-11298, but many derivatives were chemically unstable. The substitution of the C-ring phenyl was unnecessary, but some substituents such as aniline and chlorine were tolerated. The replacement of the phenyl ring with different heteroaromatic ring systems was mainly tolerated.

Synthesis

Most compounds of were prepared via reductive amination (Figure 1C, route 1), except for ORM-11298 and ORM-11863, which were prepared by aniline alkylation (Figure 1C, route 2). The reaction between the aniline and carbaldehyde derivatives could occur in the presence a strong acid at elevated temperatures. The reduction of the imine intermediate could be carried out using a suitable reducing agent, such as $NaBH_4$. The alkylation reaction in route 2 is performed in the presence of a base. The products were isolated from the reaction mixture by extraction with ethyl acetate, followed by evaporation. The starting materials used in the processes were either commercially available or could be prepared via synthetic routes (Parry et al., 2003; Ye et al., 2010). ORM-11372

was synthesized via the reductive amination of 5-(3-nitrophenyl)furan-2-carbaldehyde with the corresponding fluoroaniline, followed by the hydrogenation of the nitro group under mild conditions. Details of experiments can be found in the supplementary material (Figures S1-S14).

Cell lines and cell culture

Spodoptera frugiperda (Sf9; RRID:CVCL_0549) cells are widely used for the transient and stable expression of recombinant proteins. Here Sf9 cells were stably transfected with human NCX 1.1 and maintained in spinner flasks with TNM-FH insect medium, supplemented with 10 % foetal bovine serum, Antibiotic-Antimycotic solution, and 50 µg/ml blasticidin at 28 °C in a non-humidified, CO_2-free atmosphere. The Sf9 cell suspension was subcultured thrice a week.

Human induced pluripotent stem cell (iPSC)-derived cardiomyocytes (Cor.4U cardiomyocytes from Ncardia, Germany; RRID:CVCL_Y550) were thawed, seeded onto gelatine coated coverslips, and maintained, as described in the manufacturer's protocol. Cor4U cells express cardiac proteins including NCX1 and exhibit the relevant electrophysiology, demonstrating a potential to model human cardiac responses to drugs (Blinova et al., 2017; Huo et al., 2017).

Chinese hamster ovary (CHO) cells stably expressing either hERG1a (KCNH2; RRID:CVCL_H512; from Sophion Biosciences, Denmark) or human 5-HT_{2B} receptors (from Euroscreen, Belgium) were cultured at 37 °C in a 5 % CO_2/95 % air atmosphere in the HAM F-12 medium supplemented with 10 % foetal bovine serum (heat inactivated), 100 µg/ml hygromycin B (Invitrogen), and 100 µg/ml geneticin or 100 IU mL-1 penicillin and 100 IU mL-1 streptomycin, 25 mM HEPES, 500 µg/ml geneticin, and 250 µg/ml Zeocin®. Adhered cells were detached using either Detachin® solution or trypsin and replated twice a week. HEK 293 (RRID:CVCL_0045) and IMR-32 (from American Type Culture Collection, CCL-127; RRID:CVCL_0346) were cultured similarly, but maintained instead in Dulbecco's modified Eagle's medium or Eagle's minimum essential medium, supplemented with 10 % foetal bovine serum (heat inactivated), 100 IU mL-1 penicillin and 100 IU mL-1 streptomycin, and 25 mM HEPES, and in the case of the IMR-32 cell line, with MEM non-essential amino acids. IMR-32 cells are derived from a human neuroblastoma and endogenously express L-type calcium channels (Sher et al., 1988).

The I_{hERG} cells to be studied were harvested with Detachin solution and either diluted with a volume of CHO-cell serum-free media (supplemented with 100 IU mL-1 penicillin/streptomycin and 25 mM HEPES) to obtain cells, for which the cell density was ~4 million cells mL-1 or plated on glass coverslips and used on the following 1-2 days. HEK 293 cells were transiently transfected using lipofectamine (Invitrogen, USA), with an hSCN5A (transcript variant 2)-containing plasmid, in Optimem medium. After a 5-hour incubation period, the transfection medium was replaced with the normal growth medium. The cells were harvested by trypsinisation, centrifuged, and resuspended in the appropriate extracellular solution for performing studies the next day. CHO-5-HT_{2B} cells were plated into 96-well plates on the previous day, at a density of 40 000 cells/well, with a modified version of the growth media.

Rat ventricular cardiomyocytes

Ethical statement. All experiments were in compliance with the Guide for the Care and Use of Laboratory Animals (USA NIH publication No 85–23, revised 1996), and were approved by the Csongrád County Governmental Office for Food Safety and Animal Health, Hungary (approval No.: XIII/1211/2012). The ARRIVE guidelines were adhered to during the study (NC3Rs Reporting Guidelines Working Group, 2010).

Animals, housing, and husbandry. Six-week old male Wistar rats (200-250; RRID:RGD_13508588, obtained from a licensed supplier Toxi-coop Ltd. Hungary) were used in the study. The rats were maintained in standard rat cages (380 mm X 270 mm X 200 mm; ~1025 cm^2). The number of cage companions was 4 animals/cage. Cages were equipped with external bottle-top type lids with half-pocket wire bar lid feeders. The bedding of the cage floor was composed of aspen chips (Innovo Ltd. Hungary). The room temperature of the animal house was kept constant at 23 °C, with a humidity of 40-65%. Twelve hours of dark-light cycle was applied with a low light intensity. Food (obtained from Innovo Ltd. Hungary) and tap water were provided ad libitum to the animals. The tap water is regularly checked for any pathogens.

Cell preparation: Rats were anaesthetised with sodium thiopental (0.1 g/kg, i.p.) and injected with heparin sodium (500 IU i.v.). Hearts were rapidly excised, mounted via the aorta on a Langendorff apparatus, and retrogradely perfused at 37 °C with the Krebs-Henseleit solution for 5 min. This solution contained (in mM) 118.5 NaCl, 4 KCl, 2 $CaCl_2$, 1 $MgSO_4$, 1.2 NaH_2PO_4, 25 $NaHCO_3$, and 11.1 glucose with a solution whose pH was maintained at 7.4, when saturated with a mixture of 95% O_2 and 5% CO_2. The perfusion of the heart was continued using the Ca^{2+}-free Krebs-Henseleit solution for 10 min, and completed by the addition of 0.05% collagenase (type I), 0.05% hyaluronidase, and 200 µM $CaCl_2$, for a further 10 min. Subsequently, the left ventricular myocardium was minced and gently agitated. Dissociated cells were stored at room temperature in a solution containing (in mM) 89 KOH, 70 glutamate, 15 taurine, 30 KCl, 10 KH_2PO_4,10 HEPES, 0.5 $MgCl_2$, 11 glucose, and 0.5 EGTA and the pH was set to 7.3 using KOH. Cells were rod shaped and showed a clear striation, when external calcium levels were restored. One drop of the cell suspension was placed in a recording chamber, mounted on the stage of an inverted microscope (Olympus IX51, Olympus, Japan), and the individual myocytes were allowed to settle and adhere to the bottom of the chamber for at least 5 minutes before initiating superfusion.

Fluorescence screening assay for hNCX 1.1 inhibition

NCX reverse mode activity was stimulated via a 50% dilution of the extracellular Na^+ level using the internal pipettor of FLEXstation, a fluorescence imaging plate reader (Molecular Devices, USA), while simultaneously monitoring intracellular calcium levels. After dilution concentration of other ions remained the same, but Na^+ concentration was diluted to the half of original concentration of 172 mM to 86 mM. For Sf9 insect cells normal extracellular Na^+ ion concentration is 172 mM. Typically, 50 µl of a solution containing 150000 – 200000 Sf9-NCX cells was loaded onto each well of a 96-well plate. Cells were preincubated with the intracellular calcium dye Fluo-4 and 6, and the concentrations of the test compound (3 replicates) were determined for about 1 h at room

temperature before experimentation. The extracellular solution contained (in mM) 172 NaCl, 10 HEPES, 1 $CaCl_2$, 1.2 $MgCl_2$, 0.33 NaH_2PO_4, 5 glucose, and 5 probenecid. The pH was adjusted to 7.4 with NaOH. The extracellular Na^+ was diluted by the addition of a Na^+-free extracellular solution (containing in mM: 147 NMDG, 10 HEPES, 1 $CaCl_2$, 1.2 $MgCl_2$, 0.33 NaH_2PO_4, and 5 glucose with the pH adjusted by HCl to 7.4) induced robust and reproducible intracellular calcium elevations. The osmolarity of both solutions was adjusted to 340 – 355 mOsm in order to match the Sf9 cell media osmolarity. In each plate, the IC_{50} determination for each test compound was based on relative fluorescence changes in comparison to control and 5 mM nickel acetate-induced NCX inhibition.

Confirmatory fluorescence assay for hNCX 1 inhibition

A confirmatory hNCX1 inhibition assay was performed in Charles River Laboratories Cleveland. Briefly HEK293 cells stably expressing hNCX1 were plated in 384-well black wall, clear bottom microtiter plates and the next day loaded with Fluo-8 for 30 min at 37 ºC. A plate was inserted into a FLIPR^{TETRA} and a baseline was recorded during a pre-incubation period where test compound or vehicle in a Na^+-free HB-PS containing thapsigargin (6 µM) and FCCP (30 µM) was added to each well for ~5 min. Next the NCX1 stimulation period was recorded in which Na^+-containing HB-PS (with 2 µM thapsigargin and 10 µM FCCP) was added. The experiments were performed at room temperature. The kinetic data generated was reduced for each well to maximum relative fluorescence units (RFU) minus minimum RFU after subtracting bias based on the first sample. The mean of the max-min RFU values during the stimulation period for the 3-4 replicates at each concentration on a plate were then plotted versus concentration and fitted to a Hill equation.

Fluorescence secondary screening assays

L-type calcium channel inhibition. Undifferentiated IMR-32 cells were harvested, centrifuged and resuspended in a probenecid ringer consisting (in mM) 150 NaCl, 3 KCl, 1.2 $MgCl_2$, 1 $CaCl_2$, 20 HEPES, 5 glucose, and 2.5 probenecid (pH 7.4 adjusted with NaOH, osmolarity 320-324 mOsm). We added 0.04% Pluronic F-127 and Fluo-4 to this solution, and after incubating the cells for 30 min at room temperature, these additives were removed from the probenecid ringer via centrifugation and resuspension. The cell suspension was pipetted (250,000 cells in 75 µl per well) into a 96-well plate, into which the test compound (75 µl per well at 2,667 x the final concentration; 5 concentrations with 8 replicates) had already been added. The plate was centrifuged once (5 min, 1200 rpm) to ensure that the cells were moved to the bottom of the wells. FLEXstation was then used to measure the increase in intracellular calcium at 37 ºC, following depolarisation, which was induced by the addition (50 µl per well) of a KCl ringer containing (in mM) 200 KCl, 20 $CaCl_2$, 1.2 $MgCl_2$, 20 HEPES, and 2.5 probenecid, respectively (pH adjusted to 7.4 with KOH, with an osmolarity of 320-324 mOsm).

Serotonin 2B receptor. Changes in the intracellular calcium concentration of CHO-5-HT_{2B} cells in the probenecid ringer were measured, using Fluo-4 or Calcium 3 dyes and the FLEXstation, at 37 ºC. ORM-11372 was applied at 7 concentrations (4 replicates), 10 s after the initiating the measurement process in the agonist assay, but was preincubated (at 8 concentrations with 3 replicates) in the antagonist assay, with 10 nM 5-HT added at the 10 s time point.

Electrophysiology

Manual patch-clamp recordings[15] of membrane currents (I_{NCX}, I_{CaL}, I_{Na} and I_{hERG}) were undertaken using either an Axopatch 200B or Axopatch ID amplifier (Molecular Devices, USA), using the whole cell configuration. Cells were at least initially (except when recording I_{Na}) perfused with an extracellular solution consisting (in mM) 143 NaCl, 4 KCl, 1.8 $CaCl_2$, 1.2 $MgCl_2$, 5 glucose, and 10 HEPES (pH 7.4 with NaOH; osmolarity adjusted to 301 ± 3 mOsm). A slightly modified version was used for the rat ventricular cardiomyocytes (i.e.in mM: 144 NaCl, 0.4 NaH_2PO_4, 4.0 KCl, 1.8 $CaCl_2$, 0.53 $MgSO_4$, 5.5 glucose, and 5.0 HEPES). Patch pipettes were pulled with a P-2000 or P-97 micropipette puller (Sutter Instruments, USA) from borosilicate glass capillaries and had resistances of between 2 and 4 MΩ when filled with any of the pipette solutions (see below). The data was filtered at 1 or 2 kHz and digitised at 10 kHz with acquisition and analysis performed by use of pClamp software (versions 8-10; Molecular Devices; RRID:SCR_011323).

Measurement of NCX current (I_{NCX}). After the establishment of the whole cell configuration with hiPSC derived cardiomyocytes or rat ventricular myocytes the extracellular solution was switched to a K^+-free bath solution as described earlier (Hobai et al., 1997; Jost et al., 2013). The solution was composed (in mM) 135 NaCl, 10 CsCl, 1 $CaCl_2$, 1 $MgCl_2$, 0.2 $BaCl_2$, 0.33 NaH_2PO_4, 10 TEACl, 10 HEPES, and 10 glucose supplemented with 20 μM ouabain, 50 μM lidocaine, and 1 μM nisoldipine or 2 μM nitrendipine at pH 7.0 (osmolarity adjusted to 301 ± 3 mOsm). The pipette solution contained (in mM) 140 CsOH, 75 aspartic acid, 20 TEACl, 5 MgATP, 10 HEPES, 20 NaCl, 20 EGTA, and 10 $CaCl_2$ (pH adjusted to 7.2 with CsOH; osmolarity adjusted to 290 ± 2 mOsm). The free intracellular Ca^{2+} level in the patch pipette was 140 nM according to Maxchelator (RRID:SCR_000459) software (Bers et al., 2010).

The measurement of current in the K^+-free bath solution using a ramp voltage protocol at 20 s intervals represented the first control, after which values were measured in the presence of one or more increasing concentrations of ORM-11372, and finally upon exposure to 10 mM $NiCl_2$. The voltage protocol consisted of voltage ramps (at a rate of 100 mV/s) with a holding potential of -40 mV to 60 mV, which changed to -100 mV and then reverted back to -40 mV. I_{NCX} was defined as the Ni^{2+}-sensitive current value; however, for rat ventricular myocytes, the magnitude of the inward current (forward mode) was particularly small and variable. Therefore, to enhance the inward current and enable a solution with a certain concentration of ORM-11372 to be measured, the concentrations of the K^+-free and pipette solutions were altered. In the bath solution, the $CaCl_2$ concentration was reduced to 0.5 mM, while in the pipetted solution, the NaCl and EGTA concentrations were decreased to 5 and 10 mM, respectively. All experiments were performed at 35-37 °C. The outward human I_{NCX} inhibition current was measured at the following ORM-11372 concentrations: 3 (n = 4), 10 (n = 6), 30 (n = 4), and 100 (n = 3) nM. The concentrations used for human inward I_{NCX} current measurement were 3 (n = 4), 10 (n = 4), 30 (n = 3), and 100 (n = 2) nM. The outward I_{NCX} current in rat cardiomyocytes was measured at concentrations ranging from 1 to 1000 nM (n = 5). The inward I_{NCX} current in rats was measured in additional experiments under changed conditions, to enhance the inward I_{NCX}

current. In these experiments (n = 3), the effect of ORM-11372 was tested at a concentration of 10 nM, at which the IC_{50} and reverse I_{NCX} current values were approximately equal.

Measurement of L-type calcium current (I_{CaL}). I_{CaL} was recorded from hiPSC-derived cardiomyocytes (at room temperature, n = 2) and rat ventricular myocytes at 1 µM (n = 3; 5 cells) and at 10 µM (n = 4; 6 cells) in an extracellular solution supplemented with 3 mM of 4-aminopyridine at 37 ºC. The pipette solution used for hiPSC-derived cardiomyocytes consisted (in mM) (pH 7.2; osmolarity adjusted to 293 mOsm) 110 KCl, 40 KOH, 20 TEACI, 3 MgATP, 10 EGTA, and 5 HEPES. The composition of the pipette solution used for rat cardiomyocytes was (in mM) 125 CsCl, 20 TEACI, 5 MgATP, 10 EGTA, and 10 HEPES; the pH was adjusted to 7.2 using CsOH. I_{CaL} was evoked by a 400 ms depolarization process to 0 mV from a holding potential of -40 mV every 5 s, or in the case of the rat cardiomyocytes, by 400 ms; depolarizations to potentials ranging from -35 mV to 55 mV occurred after a prepulse to -40 mV, from the holding potential of -80 mV.

Measurement of $Na_V1.5$ current (I_{Na}). Recordings were performed on HEK cells (n = 3) that transiently expressed SCN5A at room temperature, in a bath solution containing (in mM) (pH 7.4 with N-methyl-D-glucamine; osmolarity adjusted to 300 ± 2 mOsm) of 40 NaCl, 97 L-aspartic acid, 4 KCl, 1.8 $CaCl_2$, 1 $MgCl_2$, 10 glucose, and 10 HEPES. The pipette solution contained (pH 7.2 with CsOH; osmolarity adjusted to 270 ± 3 mOsm) 130 caesium methane sulfonate, 5 $MgCl_2$, 5 EGTA, 0.1 GTP, 4 Na_2ATP, and 10 HEPES. The voltage protocol, which was repeated after each second, included of the process of hyperpolarisation, from a holding potential of –80 mV to -120 mV for 200 ms, followed by that of depolarisation to -15 mV for 10ms. The peak current values observed while applying the test pulse at -15 mV were used for analysis.

Measurement of $K_V11.1$ current (I_{hERG}). Values from hERG expressing cells (n = 4) were recorded with the standard extracellular solution at the physiological temperature and a pipette solution containing (in mM) 130 KCl, 7 NaCl, 5 EGTA, 1 $MgCl_2$, 5 Na_2ATP, and 5 HEPES (pH was set to 7.2 with KOH; osmolarity was adjusted to 290 ± 3 mOsm). I_{hERG} was evoked using a voltage protocol, which was repeatedly performed every 10s, consisting of a depolarisation step from the holding potential of –75 mV to 10 mV for 500 ms, followed by a repolarisation step to –40 mV for 500 ms. The peak tail current values at –40 mV were used for analysis.

In addition, after loading the CHO-hERG cell suspension, whole cell voltage-clamp values were recorded at room temperature on a QPatch 16x automated patch-clamp (Sophion Biosciences), in the single-hole mode. ORM-11372 solutions with concentration of 0.3 (n = 4), 1 (n = 5), 3 (n = 8), 10 (n = 8), and 30 µM (n = 8) were studied. The extracellular solution contained (in mM) 145 NaCl, 4 KCl, 2 $CaCl_2$, 1 $MgCl_2$, 10 glucose, and 10 HEPES (pH 7.4 with NaOH; osmolarity adjusted to 305 mOsm). The intracellular recording solution contained (in mM) 120 KCl, 1.75 $MgCl_2$, 5.37 $CaCl_2$, 4 Na_2ATP, 10 EGTA, and 10 HEPES (pH 7.2 with KOH; osmolarity adjusted to 295 mOsm).The voltage protocol, which was repeated every 10 s, included a 200 ms step to change the holding potential from –80 to -50 mV, to measure the leak current, and further depolarization to + 20 mV for 2 s, followed by a repolarization to –50 mV for 2 s. The hERG tail current was measured as the difference between the peak tail current amplitude during the repolarization step and leak current measurement step. Subsequently, the

voltage-dependence of the block was also assessed, by carrying out depolarization for 4 s, from –80 mV to +60 mV in 10 mV steps, before and after the addition of 20 µM ORM-11372 (n = 7). The peak tail current elicited during the 5 s repolarization step to –50 mV was measured and plotted against the preceding depolarization step voltage values.

Action Potentials. Action potentials were recorded in spontaneously beating Cor.4U cardiomyocytes in the current-clamp using the perforated patch technique and voltage-sensitive dye (di-4-ANEPPS), in a 96-well plate format. The latter ratiometric optical measurements were performed on the CellOPTIQ platform at Clyde Biosciences (Newhouse, UK). The patch-clamp measurements used the standard extracellular solution at the physiological temperature and a pipette solution containing (in mM) 122 K-gluconate, 30 KCl, 1 $MgCl_2$, and 5 HEPES (pH 7.2 with KOH; osmolarity adjusted to 290 ± 3 mOsm), and 0.24 mg/ml of amphotericin B. The patch-clamp data shown is from cardiomyocytes (n = 4) that exhibited ventricular-like action potentials, i.e. a ratio (time difference between APD_{30} and APD_{40}/time difference between APD_{70} and APD_{80}) >1.5 (Ma et al., 2011).

Selectivity Panel. Radioligand binding assays were performed at Eurofins Cerep SA (Celle L'Evescault, France), for testing the inhibition capacity of ORM-11372 (at 10 µM with 2 replicates), in over 75 targets. These included receptors (e.g. human A_1, A_{2A}, and A_3 adenosine receptors; α_1 and α_2 adrenergic receptors; human $ß_1$-$ß_3$ adrenergic receptors; human D_1, D_{2S}, D_3, $D_{4.4}$, and D_5 dopamine receptors; EGF and VEGF receptors; human M_1-M_5 muscarinic acetylcholine receptors; human 5-HT_{1A}, 5-HT_{2A}, 5-HT_{2B}, 5-HT_{2C}, 5-HT_{4e}, 5-HT_{5A}, 5-HT_6, and 5-HT_7 serotonin receptors), ion channels (5-HT_3, Ca^{2+}, K_{ATP}, K_V, SK_{Ca}, Na^+, and Cl^-), and transporters (adenosine, norepinephrine, dopamine and serotonin). Follow-up functional studies (with 5 concentrations and 2 replicates) were performed for 5-HT_{2A} and the norepinephrine transporter. Agonism and antagonism at h5-HT_{2A} was explored in recombinant HEK 293, and intracellular calcium changes were detected using fluorimetry. Norepinephrine uptake was measured by carrying out scintillation counting of [^{3}H]NE incorporated into rat hypothalamus synaptosomes.

Design and analysis for isolated heart preparations and in vivo experiments

Donor Heart Procurement: All the human hearts used for this study were obtained after legal consent was provided by organ donors in the US. The policies for donor screening and consent were the same as those established by the United Network for Organ Sharing (OPTN, 2019). Organizations supplying human tissues to AnaBios follow the standards and procedures established by the US Centers for Disease Control, and are inspected biannually by the Department of Health and Human Services. Tissue distribution is governed by internal IRB procedures and was compliance with HIPAA regulations (Edemekong et al., 2019) regarding patient privacy. All organ donor transfers to AnaBios are fully traceable and periodically reviewed by US Federal authorities. In general, AnaBios obtains donor hearts from adults aged 17–60 years old. Though some donors were trauma victims, donors with the following conditions were excluded: ejection fraction < 45%, HIV, cardiac death, HBV, congenital LQT syndrome, HCV, LOT syndrome, MRSA, downtime >20 min, ongoing infections, positive blood cultures without treatment and 48-h result data. Donor hearts from 1 male and 1 female (both 57 years old,

Table S5) were harvested using AnaBios' proprietary surgical techniques and tools, and were shipped to AnaBios via dedicated couriers. Upon arriving at AnaBios, each heart was assigned a unique identifier number that was reproduced on all relevant medical history files, data entry forms, and electronic records.

Recording of Action Potentials in Human Ventricular *Trabeculae*: Procedures used for tissue dissection and recording were similar to those described previously (Page et al., 2016). Briefly, the human heart was transferred into a dissection vessel containing a cold (4°C), fresh proprietary dissection solution. The heart was completely submerged into the dissection solution. Ventricular *trabeculae* were dissected and transferred to the recording chamber. The approach used to record action potentials (APs) is similar to that described by Page et al (Page et al., 2016). Briefly, a single tissue was mounted into the experimental chamber filled with oxygenated Tyrode's external solution, containing (in mM) 136 NaCl, 4 KCl, 0.5 $MgCl_2$, 12 $NaHCO_3$, 0.35 NaH_2PO_4, 11.1 dextrose, 1.8 $CaCl_2$, and 10 HEPES (pH 7.4). The temperature of the solution was maintained at 37°C, at a flow rate of 5 mL per minute. The tissue was allowed to equilibrate for 30-60 min, while providing stimulation (3 V, 3 ms) at a frequency of 1.0 Hz. High impedance borosilicate microelectrodes were prepared with a tip resistance of 10-20 MΩ, filled with 3 M KCl. Upon tissue impalement, the membrane potential was allowed to stabilize (typically, around -85 mV). Tissues with resting membrane potentials more positive than −75 mV were rejected. Bipolar stimulation at 1.5x threshold was applied, and recordings were obtained in the continuous mode with sampling at 20 kHz, using ADInstruments and LabChart Software. Tissue exclusion criteria included the following: (1) interruption of perfusion/oxygenation; (2) absence of APs following stimulation at baseline; (3) time frame of drug exposure not respected; (4) unstable response to stimulation at baseline; (5) resting membrane potential (RMP) > −75 mV; (6) maximal amplitude of AP (A_{MAX}) < 70 mV; and (7) AP duration at 90% repolarization (APD90) < 200ms or >450 ms. ORM-11372 was evaluated at 3 concentrations in 4 ventricular *trabeculae* derived from 2 donor hearts (n=2, two replicates). Testing concentrations were 0.1, 1, and 10 mM. Following the stabilization of each tissue, APs were collected and assessed for 31 min in the vehicle control solution (Tyrode with 0.1% DMSO), at stimulation frequencies of 1 Hz for 25min, 2Hz for 3 min, and 1Hz for 3 min. Following this vehicle control period, 3 concentrations of ORM-11372 were applied sequentially and cumulatively. Each concentration was applied for 31 min with the same stimulation sequence as in the vehicle controls.

Animal experimental design and analysis

All animal experiments were performed according to European Community Guidelines for the use of experimental animals and approved by the Finnish National Animal Experiment Board. All studies complied with the ARRIVE guidelines (NC3Rs Reporting Guidelines Working Group, 2010).

Selection of animal species: The rat is the most widely used rodent species in toxicology studies performed for drug development. The Sprague-Dawley rat strain (RRID:RGD_70508) is commonly used in the rat myocardial infarction (MI) model (Fishbein et al., 1978). However, the functional similarity between the Ca^{2+} handling proteins (including NCX) in rats (Bassani et al., 1994) and human hearts is rather low. The Ca^{2+} circulation balance in the guinea-pig and rabbit hearts are more similar to that

of a human (Milani-Nejad et al., 2014). Rabbits and humans are also known to react similarly to medication; hence, the rabbit was selected as a nonrodent species.

Housing and husbandry: Animals were monitored daily by laboratory personnel. If the general health status of an animal was significantly worsened, the animal was sacrificed with an overdose of pentobarbital. Human endpoints included no spontaneous movements and inability to drink or eat during the 24-h observation period, massive bleeding, spontaneous inflammation, missing anatomical features or swelling, and breathing difficulties. Specific pathogen-free animals were housed in half-barrier rooms where special protective clothing was required by personnel. Animal rooms were cleaned regularly 3 times per week and cages and bottles were changed at regular intervals once a week. The temperature was maintained at 22 ± 2°C and humidity at 55 ± 15%. In the light-dark cycle, lights were kept on from 06.00 to 20.00 h. Body weights of all animals were measured weekly.

Randomization and blinding: Randomization was used whenever feasible. Guinea-pigs were randomized into vehicle and ORM-11372 groups for in vitro contraction force measurement from papillary muscle. In hemodynamic studies involving rabbits, only one study group was used, according to the 3R principle. Because the experimental setup involved ascending doses in one study group, randomization was impossible. Baseline values were used as controls to reduce variability. However, the MI rat model required the inclusion of two study groups, to eliminate the effect of surgical operations. The MI study setup enabled the use of randomization. The study duration for anestetised animals is limited; hence, higher doses had to be administered, which required blinding to be performed in all *in vivo* studies. The blinding was not considered relevant, because measured absolute values and derivated parameters are not sensitive to biased interpretations.

In vitro contraction dynamics measurement

Guinea-pigs (both sex, body weight ranging 342-565 g, Dunkin Hartley, M&B A/S, Ry, Denmark) were used in the study. The animals were housed in solid bottom polycarbonate cages (Makrolon® IV, 385 x 590 x 200 mm) with stainless steel wire mesh lids, up to three animals of same sex per cage. Autoclaved aspen chips (Tapvei Ky, Kaavi, Finland) were used as bedding. A commercially available rodent SDS FD1 (P) SQC pellet diet (Special Diet Services Ltd, Witham, England) and tap water from the public supply (Espoon vesilaitos, Espoo, Finland) were available *ad libitum* in polycarbonate bottles (800-1000 ml) with plastic cabs (Scanbur A/S, Ejby, Denmark).

Guinea-pigs will be killed by a blow on the skull and the heart will be excised. Right ventricular papillary muscle will be dissected and rinsed in ice-cold Tyrode solution. Thereafter, the papillary muscle will be mounted for the measurement of twitch tension in an organ bath containing modified Tyrode solution (at 37°C) bubbled with carbogen (95% O_2, 5% CO_2). The composition of the Tyrode solution will be the following (mM): 135 NaCl, 1 $MgCl_2$ x $6H_2O$, 5 KCl, 2 $CaCl_2$ x $2H_2O$, 15 $NaHCO_3$, 1 Na_2HPO_4 x $2H_2O$, 10 glucose at pH 7.3-7.4.

The signal was acquired with a validated acquisition system ACFO v1.0 (Fision Oy, Finland). The following parameters were measured: twitch tension (Tw), rest tension (RT), time to peak tension

(TTP), and half relaxation time (HRT). At steady state, 15 twitch tensions were acquired and averaged was used for statistics.

The baseline twitch tensions were measured after a stabilization period of 20-40 min. Thereafter, vehicle (1.1% DMSO) or ORM-11372 in the Tyrode solution were superfused into the cuvette for 15 min and the effects were measured from the steady state level. All experiments were carried out at 37°C.

Experimental of myocardial infarction model

Male Sprague-Dawley rats (Harlan, Netherlands B.V.) were housed in polycarbonate cages (Makrolon® IV with stainless steel wire mesh lids). A maximum of 5 rats were housed per cage with aspen chip bedding (Tapvei Ky, Kaavi, Finland). Rats had free access to water (twice filtered, Espoon Vesi) and a rodent diet (SDS RM1 (P) SQC pelleted diet, Special Diet Services Ltd, Witham, England). The acclimation period before experiments was at least 5 days. In the myocardial infarction model, rats (7-8 weeks, 200-250 g) were randomised into either the myocardial infarction or sham groups. In this weight range, a rat is considered a young adult, when its evolution phase is characterized by slow growth and its surgical mortality is lower than that of older animals. Male rats were used to minimize the variability of the cardiac response to several stimuli (Zornoff et al., 2009).

Rats were anesthetized with a combination of ketamine (Ketalar® 50 mg/kg i.p.) and medetomidine (Domitor 250 µg/kg i.p.), intubated, and artificially ventilated with air (Ugo Basile 7025). A myocardial infarction (MI) was induced by the occlusion of the left coronary artery under aseptic conditions (Levijoki et al., 2001; Selye et al., 1960). The left coronary artery was ligated at a distance of about 2-3 mm from the origin of the aorta with a silk suture and the heart was repositioned into the chest. After ligation, the wound was closed carefully. The muscle layer was closed with soluble stitches and skin layers with insoluble stitches, followed by a partial reversal of anesthesia via the intraperitoneal administration of atipamezole (Antisedan® 0.3 -1 mg/kg i.m.). The trachea tube was removed, and the trachea and underlying muscle and skin layers were closed immediately. To prevent dehydration, rats were subcutaneously administered 5 ml of 0.9% NaCl. After surgery, rats were pain-medicated with buprenorphine for at least two days (0.05 mg/kg s.c. twice a day). For sham-operated rats, the same procedure was performed, without ligation. Rats were analysed for 7 days after the myocardial infarction (MI), for severe acute heart failure development e.g. oedema or breathing difficulties.

Hemodynamic measurements of anesthetized animals

All animals were administered multiple ascending infusion doses of ORM-11372; blinding was not possible. Systemic blood (SP) and left ventricular pressure values (LVPs) were measured with pressure transducers (SP for femoral artery: Isotec, Hugo Sachs Elektronic, Germany; a miniature pressure transducer Mikro-Tip transducer SPR-249, Millar Instruments was inserted into the left ventricle via the right carotid artery). The signal was amplified (DC-bridge amplifier type 660, Hugo Sachs Elektronik, Germany), digitised (I/O connector block type SCB-68, National Instruments, USA),

recorded, and analysed (IHME 1.0.9, Fision Ltd, Finland). Left ventricular inotropic effect (LV $+dP/dt_{max}$), relaxation (LV $-dP/dt_{min}$), and heart rate (HR) values were analysed from LVP signals.
At the end of the hemodynamic experiments, rats and rabbits were killed with an overdose of pentobarbital. Small laboratory equipments (forceps, scissors, scalpels, etc.) were sterilized in the glass bead sterilizer at 300°C for 10 sec (10 sec).
The blood pressure waveform was measured continuously in milliseconds. The blinding was not considered relevant, because the absolute value was not sensitive to biased interpretations, and all parameters are derived from of them.

Haemodynamics in MI rats: Haemodynamics were assessed 7 days after a myocardial infarction (n=6) or sham operation (n=6) as follows. Rats were anesthetized with isoflurane (2.25-2.5 %, Baxter) in carbogen (95 % O_2 and 5 % CO_2) and nitrous oxide (1:1), using a small rodent ventilator (Ugo Basile 7025, ~10 ml/kg, 60 strokes/min). The rats were infused with 0.9 % NaCl in the carotid vein at the stabilization and baseline levels. ORM-11372 was administered into MI (n=6) and sham (n=6) rats in ascending infusion doses of 1.7, 17, 167, and 417 µg/kg/min. Infusions were administered into the jugular vein of MI rats at the infusion rate of 5 ml/kg/h (Terumo TE-311, Belgium). Doses were selected based on a pilot study with healthy rats (Figure S20). The total number of animals in the study was 12+2, due to the replacement of two MI rats. One MI rat died while administering anesthesia, as infarcted animals are sensitive to anesthesia, and another MI rat was excluded due to the dosing error indicated by the bioanalysis of plasma samples (no ORM-11372 concentration observed in plasma).
After hemodynamic assessments, the anesthetized rats were killed with an overdose of pentobarbital (2 ml of Mebunat® vet 60 mg-ml per rat). The entire heart of each animal was fixed in buffered 4% formaldehyde solution, trimmed, processed, and embedded in paraffin. The hearts were cut horizontally at three different levels: apex, mid part, and base. Sections with a thickness of 4 µm were cut from each level stained with haematoxylin and eosin, for general histopathological analysis. Infarct sizes were determined using picrosirius red staining as an indicator of cardiac fibrosis, and the size was measured using Analysis Pro software. The infarct area was calculated as the percent of fibrotic tissue in the total myocardial area (mean of three levels).

Haemodynamics in rabbits: Male New Zealand white rabbits (Harlan, Netherlands B.V.) were housed individually in polycarbonate cages (Scanbur number 8 plastic cages with stainless steel door) with aspen bedding (Aspen Bricks M, Tapvei Ky, Kaavi, Finland). The acclimation period before experiments was at least 21 days. Rabbits weighing 2.0-2.3 kg (age 10-12 weeks) were used for hemodynamically assessing ORM-11372 (no randomisation, baseline values as own control). The diet provided to rabbits was SDS Stanrab (P) SQC pelleted (Special Diet Services Ltd, Witham, England). Water was provided ad libitum in polycarbonate bottles (750 ml).
Rabbits (n=5) were sedated with intravenously (marginal vein) injected diazepam (2 mg/kg, Diapam®, Orion Pharma). Anesthesia was inducted with intravenous s-ketamine (10-20 mg/kg Ketanest-S®, Pfizer) and maintained with a s-ketamine intravenous infusion (15-80 mg/kg/h). Animals were placed on a heating table (+38°C) and tracheas were cannulated. Rabbits were ventilated via a rodent

ventilator (Ugo Basile type 7025, Hugo Sachs Elektronik, Germany; respiratory volume 10 ml/kg, 30 strokes per min for rabbits). ORM-11372 was administered into the jugular vein at an infusion rate of 10 ml/kg/h (Terumo TE-311, Belgium), at infusion doses of 17, 167, and 833 µg/kg/min.

Blood sampling for bioanalysis

At the end of each infusion process, blood samples (300-500 µl) added to a chilled EDTA polypropylene tube (CapiJect®, Terumo) and centrifuged (4000 rpm, 10 min, at 4°C). Plasma was immediately frozen in polypropylene tubes and stored at –20°C. ORM-11372 was extracted from plasma samples using a liquid–liquid extraction process and analysed using liquid chromatography–tandem mass spectrometry (Agilent Technologies series 1100 liquid chromatographic system and a Sciex LC-MS/MS API 4000 mass spectrometry). The lower limit of quantification for the plasma concentration of ORM-11372 was 32.0 ng/ml. Plasma protein binding in ORM-11372 was assessed using the TRANSIL High Sensitivity kit, as per the manufacturer's instructions (Sovicell, GmbH, Germany).

Materials

Study substance: ORM-11372 was synthetized by Orion Pharma. To perform in vitro experiments, ORM-11372 was dissolved in dimethyl sulphoxide (DMSO), to obtain a 10 mM stock solution. Spiking solutions were prepared daily by diluting the stock solution with DMSO, and used to prepare the final drug solutions with certain concentrations by diluting them with extracellular solutions (the vehicle concentration was either 0.1 or 0.3 %). The solubility of ORM-11372 in saline and 5% glucose solutions used for *in vivo* dosing were were 5.3 mg/ml and 5.4 mg/ml, respectively. ORM-11372 was soluble in 10 – 100 µg/ml of phosphate buffer (in pH 7.4). ORM-11372 has the following drug like properties: the number of hydrogen bond acceptors is 1 (<10) and donors is 3 (<5), molecular weight of free base is 282 (<500), and the predicted logP value is less than 5 (ADMET Predictor: 3.95, MOE: 3.413, QikProp: 3.974).

Chemicals: Isoflurane (Forane®, Baxter), atipamezole (Antisedan®, Orion Pharma), medetomidine (Domitor®, Orion Pharma, ketamine (Ketalar®, Pfizer Oy Animal Health, lipofectamine (Invitrogen, USA), hygromycin B (Invitrogen), buprenorphine (Temgesic®, INDIVIOR UK Ltd). All other chemicals and cell culture media were obtained from Sigma-Aldrich.

Cell lines and cell culture: NCX 1.1 was cloned and plasmid was constructed by Orion Pharma *Spodoptera frugiperda* (Sf9) cells (ATCC), human induced pluripotent stem cell (iPSC) derived cardiomyocytes (Cor.4U cardiomyocytes from Ncardia, Germany), Detachin™ Cell Detachment Solution, Genlantis), HEK 293 cells and IMR-32 human neuroblastoma cells (ATCC), CHO cells hERG1a (KCNH2; Sophion Biosciences, Denmark), CHO cells human 5-HT2B receptors (Euroscreen, Belgium), hSCN5A plasmid (OriGene Technologies Inc., Rockville, MD, USA).

Data and Statistical Analysis

Data Analysis of human *trabeculae*: For each frequency tested, the last 30 APs acquired at the end of the period were averaged for vehicle controls, for each ORM-11372 solution with a certain concentration. Analysis at 1 Hz included only the last 30 APs from the initial 25 min incubation period. The following AP parameters and pro-arrhythmia variables were analysed offline upon the completion

of recordings: RMP (mV), AMAX (mV), AP duration at percent repolarization (APD30, APD50, APD90) (ms), short term variability analysis of AP duration (STV), triangulation (APD90-APD30).

STV was calculated as the beat-to-beat variability in repolarization from APD90 Poincare plots over a 30 sec duration. STV for APD90 was calculated as follows: $STV = \sum|APDn+1-APDn|/(30\times\sqrt{2})$, where APD (n) and APD(n+1) are the APDs for the nth AP and the following AP, respectively.

The effects of ORM-11372 were quantified relative to the data collected during the vehicle control period. Threshold values for changes over the baseline control for APD30, APD50, APD90, triangulation, and STV at 1 and 2 Hz pacing frequencies have been determined in a previous validation study (Page et al., 2016). Results are expressed as mean ± standard error values of the mean (SEM).

The data and statistical analysis of in vitro and in vivo studies comply with the recommendations for experimental design and analysis in pharmacology.(Curtis et al., 2018). Statistical analysis were done only where number of independent samples was 5 or more. A p-value of <0.05 was considered to be significant. Two-way repeated measures ANOVA were used for the analysis of the papillary muscle and myocardial infarction models. One-way repeated measures ANOVA was used for the rabbit hemodynamic study. The Sidak posthoc-test was run only if the F-value was statistically significant, and there was no significant variance in homogeneity. Data is presented as mean ± SEM. Prism 8.0.2 (GraphPad Software Inc., San Diego, CA, USA; RRID:SCR_002798) was used for statistical analysis.

Nomenclature of Targets and Ligands

Key protein targets and ligands in this article are hyperlinked to corresponding entries in http://www.guidetopharmacology.org, the common portal for data from the IUPHAR/BPS Guide to PHARMACOLOGY (Harding et al., 2018), and are permanently archived in the Concise Guide to PHARMACOLOGY 2019/20 (Alexander et al., 2019).

Results

ORM-11372 concentrations dependently inhibited the increase in intracellular calcium in insect cell line expressing human NCX1.1. The insect cell line was used as the screening assay. The IC_{50} for the inhibition of NCX in the reverse mode was 6.2±0.4 nM.

The potency of ORM-11372 for NCX was subsequently studied using the whole-cell patch-clamp technique in human iPS-derived cardiomyocytes (hiPSC-CMs; Figure 3) and rat ventricular cardiomyocytes (Figure 4). The solutions and experimental protocol used to measure the bidirectional NCX current (I_{NCX}) was identical for both preparations. As shown in Figure 3A, the current was recorded in response to repetitive voltage ramp pulses first in a K^+-free bath solution after blocking Na^+, Ca^{2+}, K^+, and Na^+/K^+ pump currents, to yield the baseline, and during the addition of ORM-11372. Finally, when the highest concentration of ORM-11372 had reached a steady state, 10 mM $NiCl_2$ was added to completely block I_{NCX}. Examples of individual trace currents under different conditions are shown for a hiPSC-CM in Figure 3B and for a rat cardiomyocyte in Figure 4A. ORM-11372 decreased both the outward and inward currents. The IC_{50} values for the outward and inward I_{NCX} (i.e. the Ni^{2+}-sensitive current) of hiPSC-CMs were 4.8 and 5.6 nM, respectively (Figure 3C). In rat primary ventricular cardiomyocytes, the magnitude of outward I_{NCX} (the reverse mode) with an IC_{50} of 11.3 nM (Figure 4B) was reduced in an ORM-11372 concentration-dependent manner. It was difficult to

record inward I_{NCX} (the forward mode) from rat cardiomyocytes; hence, the experimental conditions were altered, to enhance its magnitude (see Methods). At 10nM, the approximate IC_{50} on the outward I_{NCX}, ORM-11372 inhibited inward I_{NCX} by 53.8±3.9 %.

Comparison with known NCX inhibitors

Further confirmation of the inhibitory effects of ORM-11372 was sought in the hNCX1 fluorescence calcium flux assay available at Charles River. In experimental conditions increasing intracellular calcium (by the presence of thapsigargin and FCCP) and eliciting NCX forward mode activity (switching from Na^+-free to Na^+-containing buffer), ORM-11372 concentration-dependently inhibited the calcium efflux signal (Figure 5A) with an IC_{50} of 142 nM and 164 nM (0.3 % and 1 % DMSO respectively; NS). The hNCX1 antagonist of five other compounds was also assessed in this assay. ORM-11372 was the most potent inhibitor (Figure 5B) followed by ORM-10962 (Figure 5C), ORM-10103, SEA0400, KB-R7943, and lastly SN-6 whose IC_{50} appears >100 µM.

Selectivity

The functional selectivity of ORM-11372 towards the L-type Ca^{2+} channel was first tested with the IMR-32 neuroblastoma cell line, using fluorometric images of intracellular changes in calcium levels. Depolarisation of undifferentiated IMR-32 cells by KCl addition induced an increase in intracellular calcium levels, which can be suppressed by preincubation with verapamil or the 1,4-dihydropyridine nicardipine (Sher et al., 1988). L-type calcium channels mediated changes in intracellular calcium levels, and these were concentration dependently inhibited by an ORM-11372 solution with an IC_{50} of 6.1 µM. Further electrophysiological studies were then performed with hiPSC-CMs and rat ventricular cardiomyocytes. The inward I_{CaL} was reduced by 1 µM ORM-11372 at 0 mV by 14.1 % in hiPSC-CMs (Figure 6A), and a 7.8 % inhibition was observed in rat cardiomyocytes (Figure S16A-B; Individual inhibition values at 1 and 10 µM are shown in Table S3 and S4, respectively). However, when rat ventricular cardiomyocytes were exposed to ORM-11372 at a concentration of 10 µM, I_{CaL} was significantly decreased (Figure S16C). I_{CaL} inhibition exhibited voltage dependency, and was greater (59-69 % versus 36-39 %) at more negative activating test potentials (-35 to -20 mV versus 0 to 40 mV).

The effect of ORM-11372 on other cardiac ion channel currents were investigated. The reduction in the human $K_V11.1$ current (I_{hERG}) was initially examined using stably expressing cells on an automated patch-clamp instrument, and then with the manual patch-clamp. ORM-11372 concentration dependently inhibited I_{hERG} (Figure 6B); IC_{50} values were 19.2 and 10.0 µM, using the automated and manual patch-clamp methods, respectively (Figure S15A). ORM-11372 significantly altered the voltage dependency of the I_{hERG} activation curve (Figure S15C) and displayed significant voltage dependent blockage. While I_{hERG} inhibition was minimal at –30 and –20 mV, inhibition increased markedly at –10 and 0 mV, and reached a steady state between 10 and 60 mV, *i.e.* at potentials where the channels were fully activated (Figure S15D). Additionally, ORM-11372 concentration dependently inhibited human the $Na_V1.5$ current (Figure 6C), with an IC_{50} value of 23.2 µM.

ORM-11372 increased twitch tension by 146 ± 32% vs. 7 ± 5% in vehicle group (Figure 6D), but did not increase rest tension (-8 ± 2% vs. -10 ± 1% in vehicle, Figure 6E), did not affect time to peak (-4

± 1% vs. -5 ± 2% in vehicle, Figure 6F) nor half relaxation time (8 ± 9% vs. 11 ± 4% in vehicle, Figure 6G).

The selectivity profile of ORM-11372 was additionally evaluated in binding assays for a diverse panel of targets. While minor effects such as those for the Na^+/K^+-ATPase or ryanodine receptor (11 % and 15 % inhibition) were seen, with a screening concentration of 10 µM, specific ligand binding inhibition was significant(i.e. >50 %) at the peripheral benzodiazepine receptor, imidazoline I_2 receptor, serotonin 2_A and 2_B receptors, and norepinephrine transporter. The latter three targets were studied functionally. The uptake of norepinephrine into rat hypothalamus synaptosomes was inhibited by ORM-11372 in a concentration-dependent manner; the IC_{50} value was 1.7 µM. Neither agonism nor antagonism was seen with ORM-11372 (maximum concentration: 10 µM) at 5-HT_{2A}. Similarly, no agonism was evident at 5-HT_{2B}; however, 10 µM ORM-11372 moderately inhibited (38 %) the 5-HT_{2B}-mediated increase in intracellular calcium evoked by 10 nM serotonin.

Human ventricular *trabeculae*

ORM-11372 caused no significant changes in APD_{30}, APD_{50}, and APD_{90} values up to a concentration of 10 µM, at both 1 and 2 Hz pacing frequencies. However, there was a trend in the reduction in APD, particularly APD_{30}, at 1Hz (Figure S17); this seemingly contrasts with the significant shortening of hiPSC-CM APD by ORM-11372 (at 0.1 or 0.3 µM; Figure S18). As expected, the effect of the positive control (0.1 µM dofetilide) was observed in *trabeculae* tested with ORM-11372 (Figure 7; individual values are shown in Figure S17 (Page et al., 2016; Qu et al., 2017). Moreover, ORM-11372 showed no effects on STV and triangulation, two pro-arrhythmia markers that are used to identify pro-arrhythmic risk (Page et al., 2016; Qu et al., 2017), at a pacing rate of 1 or 2 Hz, at any tested concentration (Individual values in Figure S19). However, the addition of 0.1 µM dofetilide to the *trabeculae* tested with ORM-11372 increased STV and triangulation (Figure S18). Taken together, these data clearly suggest that ORM-11372 can be classified as devoid of pro-arrhythmic risk.

In vivo haemodynamics in rat myocardial infarction (MI) model

Infarcted areas were 14.5±1.8% and 1.1±0.6% in the MI and sham-operated groups, respectively (Figure S20). Percentage changes are calculated from absolute values. Infarctions caused the baseline of positive inotropic effect and relaxation to be reduced by 38% and 23%, respectively. Heart rates (-3%) were unaffected, but systemic arterial pressure reduced by 20%.

In MI rats, ORM-11372 improved maximally positive inotropic effect by 18 ± 6% and by 31 ± 6% in sham rats (Figure 8A). Maximal effects were observed at the highest infusion dose of 417 µg/kg/min, corresponding to free plasma concentrations of 6.7 ± 2.5 and 4.9 ± 0.4 nM. At the lowest infusion dose of 1.7 µg/kg/min, ORM-11372 improved relaxation levels in the MI group by 24 ± 2% (Figure 8B). ORM-11372 maximally reduced the heart rate by 14 ± 4% (SHAM -2 ± 2%; Figure 8C). ORM-11372 had no systemic arterial blood pressure effects in the MI or SHAM groups (Figure 8D).

In vivo haemodynamics in rabbits

ORM-11372 induced a 35 ± 8% (calculated from absolute values) statistically significant increase in cardiac contractility in healthy rabbits, at an infusion rate of 833 µg/kg/min (Figure 9A). At rates of

17-833 µg/kg/h, ORM-11372 infusions did not have any effects on cardiac relaxation (Figure 9B), heart rate (Figure 9C), or systolic blood pressure (Figure 9D) in healthy rabbits.

Discussion

Although the first NCX inhibitor, XIP, was a peptide, it enabled us to study the role of NCX under physiological and pathological conditions in cells and isolated tissues (Hobai et al., 1997). However, it took 20-30 min for NCX to be inhibited; it also inhibited SERCA and PMCA (Enyedi et al., 1993). The next important step was the isolation and characterization of the naturally occurring NCX inhibitor (NCX_{IF}) (Hiller et al., 2000). It was the first specific, cell membrane-penetrating NCX inhibitor (Shpak et al., 2003), but the structure of NCX_{IF} was not published.

The first generation compounds (Table S1) that were specifically targeted to inhibit NCX were used as pharmacological tool to assess the inotropic mechanisms of various drugs like cardiac glycosides (Ruch et al., 2003; Tanaka et al., 2007) and insulin (Hsu et al., 2006). The potency of the first generation NCX inhibitors was modest and selectivity between NCX and other membrane currents was poor, especially towards the L-type Ca^{2+} current (Birinyi et al., 2005). SEA0400 was positively inotropic in rats, but not in rabbits (Farkas et al., 2008), in which the role of NCX is similar to that of humans. For the second generation NCX inhibitor ORM-10103 (Koskelainen et al., 2003), the selectivity between NCX and other currents were improved (Kormos et al., 2014). The following molecule ORM-10962 (Otsomaa et al., 2004) exhibits even better potency and more improved solubility (Kohajda et al., 2016). Discovery of ORM-11372 created the ground for the third generation NCX inhibitors with the unique structure combined with improved drug likeness.

ORM-11372 inhibited NCX 1.1 reverse and forward mode currents with a similar potency in both human iPS and rat cardiomyocytes. Furthermore, the inhibition of human and rat NCX 1.1 currents were shown to be of the same magnitude (IC_{50} were 5 vs 10 nM). NCX 1.1 expression has been demonstrated in iPS-CMs (Fine et al., 2013; Kodama et al., 2019). To our knowledge, the presence or absence of the other NCX subtypes in hiPS has not yet been reported. Furthermore, NCX 1.1 expression is tissue specific (Lee et al., 1994); it can be stated that ORM-11372 is a potent and selective NCX 1.1 inhibitor compared to other cardiac ion channels, but NCX subtype selectivity is unknown. NCX have specialized role in excitation-contraction coupling. Cell specific regulation of NCX1 expression is due to cardiac specific promoter which leads to very high expression of NCX1.1 in cardiac tissue (Nicholas et al., 1998). Hence, the effect of ORM-11372 is cardiac specific. In earlier studies, it was speculated that positive inotropic effects could be attributable to the asymmetrical blocking of NCX (Oravecz et al., 2018). ORM-11372 induced positive inotropy in healthy and myocardial infarcted rats, although it symmetrically inhibited both inward and reverse NCX currents. In rat plasma, the effective free concentration range of ORM-11372 was from 4 to 300 nM (Fig S20), corresponding to the NCX inhibition range of IC_{25} to IC_{80} in rat cardiomyocytes (Fig 4C). ORM-11372 induced positive inotropy even *in vivo*, in the healthy rabbits, in contrast to SEA0400 (Farkas et al., 2008). The fact that the ORM-11372 NCX inhibitor is over 10 times more potent than SEA0400 explains its positive inotropic effect in rabbits. This was also confirmed in hNCX1-HEK assay (Fig 5). ORM-11372 increased twitch tension (Figure 6D)

which indicates increased SR load. Furthermore, unlike SEA0400, ORM-11372 inhibited NCX 1.1 current selectively, and other cardiomyocyte currents were negligibly inhibited.

ORM-11372 had no effect on relaxation levels in normal rats and rabbits, but at the lowest dose, it improved relaxation levels in myocardial infarcted rats. Rat hemodynamics is subject to limitation of the fact that rat cardiomyocyte relaxation depends less on NCX and more on the other Ca^{2+} handling mechanisms. An earlier study conducted *in vitro* using SEA0400 showed that NCX inhibition caused a deterioration in transient Ca^{2+} levels, but not mechanical relaxation (Szentandrassy et al., 2008). An *ex vivo* study using an isolated perfused rat heart with artificial ionic modification demonstrated that NCX inhibition also deteriorated mechanical relaxation levels (Chen et al., 2012). Yet, it must be emphasized that the earlier studies were performed using the weaker and less selective inhibitor SEA0400 (Table 1), under artificial conditions. ORM-11372 did not affected relaxation in guinea-pig papillary muscle (Figure 6G) neither *in vivo* rabbits due to the activation of compensative Ca^{2+} handling mechanisms in cardiomyocytes, as increased intracellular Ca^{2+} levels enhance SERCA and / or PMCA activity. Furthermore, ORM-11372 had no effects on rest tension (Figure 6E) indicating no increase in diastolic calcium. ORM-11372 did not either affect time to peak (Figure 6F) which demonstrate that calcium release from ryanodine receptors is normal. Our findings are in line with the study using NCX_{IF}. Hemodynamic models of present study were exclusively done on male rats and rabbits which might introduce potential bias due to sex differences. Our results with human *Trabeculae* and guinea-pig papillary muscle did not show any differences between sexes although number of experiments are low. However, differences in calcium handling activity and NCX expression level in cardiomyocytes has been published between sexes, age and regional expression of NCX (Janczewski et al., 2010). Therefore, the role of NCX in calcium handling between sexes should be systematically furher explored.

ORM-11372 selectively inhibited I_{NCX} over a $K_v11.1$ current, and provided a safety margin (ratio ≥ 2000) of well beyond 30-fold, which was considered adequate for ensuring an acceptable degree of safety from arrhythmogenesis (Redfern et al., 2003). Results were also confirmed in human ventricular tissue. Furthermore, ORM-11372 can be classified as being non-pro-arrhythmic in humans.

Although the NCX current seems to be crucial for beat generation (Groenke et al., 2013), even a small NCX current is enough to maintain the heart beat (Gao et al., 2013). In the present study, ORM-11372 had no effects on heart rate *in vivo* in rats or rabbits. Up to 80% NCX can be inhibited without any effects on the heart rate (Figure S20). In vascular arterial cells, NCX contributes to the maintenance of the myogenic tone (Zhang et al., 2010). In a manner similar to SEA0400 (Yatabe et al., 2015), ORM-11372 had no effects on systolic blood pressure. The aforementioned pharmacological properties resulted in unique positive inotropic effects without without the risk of hypotension, increase in heart rate, or impairment of left ventricular relaxation.

During the discovery of ORM-11372, multible iterative DMTA-cycles (Design, Make, Test, Analyse) of optimization (Andersson et al., 2009) were performed in coherence with the 3R principles, using the protein and cell based *in vitro* methods, before section of the compound for *in vivo* studies. Group size was optimized, but was big enough for obtaining reliable results. Animals were also allowed to become habituated to the procedures and the necessary analgesia was used. Rats and rabbits were

selected to ensure similar responses and improved prediction capabilities from *in vitro* to *in vivo* studies, which ultimately would be translated into better efficacy and safety in human studies. To improve pharmacokinetic and pharmacodynamic interpretation, the plasma levels of ORM-11372 were monitored at the end of each pharmacodynamic experiment.

The ORM-11372 scaffold was shown to have critical bridged aniline structure with hydrogen donor property between the A and the B ring systems (Figure 1 and 2). The 1st and the 2nd generation NCX inhibitors lack the hydrogen bond donor in their scaffold. Furthermore, the activity of the ORM-11372 series exhibited better potency in the screening assay than the known NCX inhibitors (Table S1 and S2). This indicates that an additional specific binding interaction was identified between the ligand and NCX protein. However, the finding remains speculative due to the lack of other experimental evidence e.g. protein-ligand crystal structure. The crystal structure of the mammalian NCX and its splice variants are still unavailable, though the crystal structure of the NCX protein of archaebacterial *Methanococcus jannaschii* was published in 2012 (Liao et al., 2012). There are known structural differences between the prokaryotic and eukaryotic NCX proteins that might lead to differences in the potential binding pockets and selectivity (John et al., 2013; Khananshvili, 2014). Thus, evidence regarding the binding pocket for ORM-11372, as well as for the other NCX inhibitors is yet to be uncovered.

Conclusions

Thus, it can be concluded that ORM-11372 is the first in a class of the third generation of NCX 1.1 inhibitors with a unique scaffold and improved profile. ORM-11372 is the most potent and selective reported NCX 1.1 inhibitor. ORM-11372 selectively inhibits cardiac NCX 1.1 current and induces positive inotropic effects in healthy and myocardial infarcted rats, as well as in rabbits. ORM-11372 has a better hemodynamic profile and similar positive inotropic effects, as compared to dobutamine, but did not cause an increase in heart rate or decrease in systolic blood pressure. Intrestingly, at a low dose, ORM-11372 improved relaxation in the myocardial infarction model. Studies involving human tissues support the classification of ORM-11372 as a non-pro-arrhythmic inhibitor.

Thus, ORM-11372 can be used as a research tool by researchers, to further study the role and function of NCX1.1 *in vitro* and *in vivo*.

Acknowledgements

We thank Dr Arto Karjalainen, a pioneer of medicinal chemistry, for providing his everlasting support as a mentor. We also wish to thank the late Dr Heimo Haikala, for inspiring us and initiating research regarding NCX inhibitors at Orion Pharma.

The study of primary cardiomyocytes outlined in this manuscript was supported by grants from the National Research, Development and Innovation Office (K-119992, PD-125402, FK-129117, and a GINOP-2.3.2-15-2016-00006), the Ministry of Human Capacities, Hungary (20391-3/2018/FEKUSTRAT and EFOP-3.6.2-16-2017-00006), the János Bolyai Research Scholarship of the Hungarian Academy of Sciences (for NN) and the Hungarian Academy of Science.

Conflicts of interest

The following are or were employees of Orion: LO, JL, GW, HC, APK, KS, TK, SEP, PF, AH and may own Orion Corporation stocks and shares. NAG, AG, PEM and GP are employees of AnaBios Corporation and may own AnaBios stocks and shares.

Open research (DATA AVAILABILITY STATEMENT)

The data that support the findings of this study are available from the corresponding author upon reasonable request. Some data may not be made available because of privacy or ethical restrictions.

Declaration of transparency and scientific rigour

This Declaration acknowledges that this paper adheres to the principles for transparent reporting and scientific rigour of preclinical research as stated in the *BJP* guidelines for Design and Analysis, and Animal Experimentation, and as recommended by funding agencies, publishers and other organisations engaged with supporting research.

References

Alexander, S. P. H., Kelly, E., et al. (2019). THE CONCISE GUIDE TO PHARMACOLOGY 2019/20: Transporters. *Br J Pharmacol, 176 Suppl 1*, S397-S493. doi:10.1111/bph.14753

Andersson, S., Armstrong, A., et al. (2009). Making medicinal chemistry more effective--application of Lean Sigma to improve processes, speed and quality. *Drug Discov Today, 14*(11-12), 598-604. doi:10.1016/j.drudis.2009.03.005

Bassani, J. W., Bassani, R. A., et al. (1994). Relaxation in rabbit and rat cardiac cells: species-dependent differences in cellular mechanisms. *J Physiol, 476*(2), 279-293. doi:10.1113/jphysiol.1994.sp020130

Bers, D. M., Despa, S. (2006). Cardiac myocytes Ca2+ and Na+ regulation in normal and failing hearts. *J Pharmacol Sci, 100*(5), 315-322.

Bers, D. M., Patton, C. W., et al. (2010). A practical guide to the preparation of Ca(2+) buffers. *Methods Cell Biol, 99*, 1-26. doi:10.1016/B978-0-12-374841-6.00001-3

Birinyi, P., Acsai, K., et al. (2005). Effects of SEA0400 and KB-R7943 on Na+/Ca2+ exchange current and L-type Ca2+ current in canine ventricular cardiomyocytes. *Naunyn Schmiedebergs Arch Pharmacol, 372*(1), 63-70. doi:10.1007/s00210-005-1079-x

Blinova, K., Stohlman, J., et al. (2017). Comprehensive Translational Assessment of Human-Induced Pluripotent Stem Cell Derived Cardiomyocytes for Evaluating Drug-Induced Arrhythmias. *Toxicol Sci, 155*(1), 234-247. doi:10.1093/toxsci/kfw200

Chen, Y., Payne, K., et al. (2012). Inhibition of the sodium-calcium exchanger via SEA0400 altered manganese-induced T1 changes in isolated perfused rat hearts. *NMR Biomed, 25*(11), 1280-1285. doi:10.1002/nbm.2799

Curtis, M. J., Alexander, S., et al. (2018). Experimental design and analysis and their reporting II: updated and simplified guidance for authors and peer reviewers. *Br J Pharmacol, 175*(7), 987-993. doi:10.1111/bph.14153

Edemekong, P. F., Haydel, M. J. (2019). Health Insurance Portability and Accountability Act (HIPAA). In *StatPearls*. Treasure Island (FL).

Enyedi, A., Penniston, J. T. (1993). Autoinhibitory domains of various Ca2+ transporters cross-react. *J Biol Chem, 268*(23), 17120-17125.

Farkas, A. S., Acsai, K., et al. (2008). Na(+)/Ca(2+) exchanger inhibition exerts a positive inotropic effect in the rat heart, but fails to influence the contractility of the rabbit heart. *Br J Pharmacol, 154*(1), 93-104. doi:10.1038/bjp.2008.83

Fine, M., Lu, F. M., et al. (2013). Human-induced pluripotent stem cell-derived cardiomyocytes for studies of cardiac ion transporters. *Am J Physiol Cell Physiol, 305*(5), C481-491. doi:10.1152/ajpcell.00143.2013

Fishbein, M. C., Maclean, D., et al. (1978). Experimental myocardial infarction in the rat: qualitative and quantitative changes during pathologic evolution. *Am J Pathol, 90*(1), 57-70.

Gao, Z., Rasmussen, T. P., et al. (2013). Genetic inhibition of Na+-Ca2+ exchanger current disables fight or flight sinoatrial node activity without affecting resting heart rate. *Circ Res, 112*(2), 309-317. doi:10.1161/CIRCRESAHA.111.300193

Geramipour, A., Kohajda, Z., et al. (2016). The investigation of the cellular electrophysiological and antiarrhythmic effects of a novel selective sodium-calcium exchanger inhibitor, GYKB-6635, in canine and guinea-pig hearts. *Can J Physiol Pharmacol, 94*(10), 1090-1101. doi:10.1139/cjpp-2015-0566

Groenke, S., Larson, E. D., et al. (2013). Complete atrial-specific knockout of sodium-calcium exchange eliminates sinoatrial node pacemaker activity. *PLoS One, 8*(11), e81633. doi:10.1371/journal.pone.0081633

Harding, S. D., Sharman, J. L., et al. (2018). The IUPHAR/BPS Guide to PHARMACOLOGY in 2018: updates and expansion to encompass the new guide to IMMUNOPHARMACOLOGY. *Nucleic Acids Res, 46*(D1), D1091-D1106. doi:10.1093/nar/gkx1121

Hilgemann, D. W., Matsuoka, S., et al. (1992). Steady-state and dynamic properties of cardiac sodium-calcium exchange. Sodium-dependent inactivation. *J Gen Physiol, 100*(6), 905-932.

Hiller, R., Shpak, C., et al. (2000). An unknown endogenous inhibitor of Na/Ca exchange can enhance the cardiac muscle contractility. *Biochem Biophys Res Commun, 277*(1), 138-146. doi:10.1006/bbrc.2000.3645

Hobai, I. A., Khananshvili, D., et al. (1997). The peptide "FRCRCFa", dialysed intracellularly, inhibits the Na/Ca exchange in rabbit ventricular myocytes with high affinity. *Pflugers Arch, 433*(4), 455-463. doi:10.1007/s004240050300

Hsu, C. H., Wei, J., et al. (2006). Cellular mechanisms responsible for the inotropic action of insulin on failing human myocardium. *J Heart Lung Transplant, 25*(9), 1126-1134. doi:10.1016/j.healun.2006.05.010

Huo, J., Kamalakar, A., et al. (2017). Evaluation of Batch Variations in Induced Pluripotent Stem Cell-Derived Human Cardiomyocytes from 2 Major Suppliers. *Toxicol Sci, 156*(1), 25-38. doi:10.1093/toxsci/kfw235

Iwamoto, T., Inoue, Y., et al. (2004). The exchanger inhibitory peptide region-dependent inhibition of Na+/Ca2+ exchange by SN-6 [2-[4-(4-nitrobenzyloxy)benzyl]thiazolidine-4-carboxylic acid ethyl ester], a novel benzyloxyphenyl derivative. *Mol Pharmacol, 66*(1), 45-55. doi:10.1124/mol.66.1.45

Iwamoto, T., Kita, S. (2006). YM-244769, a novel Na+/Ca2+ exchange inhibitor that preferentially inhibits NCX3, efficiently protects against hypoxia/reoxygenation-induced SH-SY5Y neuronal cell damage. *Mol Pharmacol, 70*(6), 2075-2083. doi:10.1124/mol.106.028464

Janczewski, A. M., Lakatta, E. G. (2010). Modulation of sarcoplasmic reticulum Ca(2+) cycling in systolic and diastolic heart failure associated with aging. *Heart Fail Rev, 15*(5), 431-445. doi:10.1007/s10741-010-9167-5

John, S. A., Liao, J., et al. (2013). The cardiac Na+-Ca2+ exchanger has two cytoplasmic ion permeation pathways. *Proc Natl Acad Sci U S A, 110*(18), 7500-7505. doi:10.1073/pnas.1218751110

Jost, N., Nagy, N., et al. (2013). ORM-10103, a novel specific inhibitor of the Na+/Ca2+ exchanger, decreases early and delayed afterdepolarizations in the canine heart. *Br J Pharmacol, 170*(4), 768-778. doi:10.1111/bph.12228

Kaese, S., Bogeholz, N., et al. (2017). Increased sodium/calcium exchanger activity enhances beta-adrenergic-mediated increase in heart rate: Whole-heart study in a homozygous sodium/calcium exchanger overexpressor mouse model. *Heart Rhythm, 14*(8), 1247-1253. doi:10.1016/j.hrthm.2017.05.001

Khananshvili, D. (2013). The SLC8 gene family of sodium-calcium exchangers (NCX) - structure, function, and regulation in health and disease. *Mol Aspects Med, 34*(2-3), 220-235. doi:10.1016/j.mam.2012.07.003

Khananshvili, D. (2014). Sodium-calcium exchangers (NCX): molecular hallmarks underlying the tissue-specific and systemic functions. *Pflugers Arch, 466*(1), 43-60. doi:10.1007/s00424-013-1405-y

Kodama, M., Furutani, K., et al. (2019). Systematic expression analysis of genes related to generation of action potentials in human iPS cell-derived cardiomyocytes. *J Pharmacol Sci, 140*(4), 325-330. doi:10.1016/j.jphs.2019.06.006

Kohajda, Z., Farkas-Morvay, N., et al. (2016). The Effect of a Novel Highly Selective Inhibitor of the Sodium/Calcium Exchanger (NCX) on Cardiac Arrhythmias in In Vitro and In Vivo Experiments. *PLoS One, 11*(11), e0166041. doi:10.1371/journal.pone.0166041

Kohajda, Z., Toth, N., et al. (2019). Novel Na(+)/Ca(2+) Exchanger Inhibitor ORM-10962 Supports Coupled Function of Funny-Current and Na(+)/Ca(2+) Exchanger in Pacemaking of Rabbit Sinus Node Tissue. *Front Pharmacol, 10*, 1632. doi:10.3389/fphar.2019.01632

Kormos, A., Nagy, N., et al. (2014). Efficacy of selective NCX inhibition by ORM-10103 during simulated ischemia/reperfusion. *Eur J Pharmacol, 740*, 539-551. doi:10.1016/j.ejphar.2014.06.033

Koskelainen, T., Otsomaa, L., et al. (2003). Finland Patent No. WO2003006452A1. F. Orion Corporation.

Lee, S. L., Yu, A. S., et al. (1994). Tissue-specific expression of Na(+)-Ca2+ exchanger isoforms. *J Biol Chem, 269*(21), 14849-14852.

Levijoki, J., Pollesello, P., et al. (2001). Improved survival with simendan after experimental myocardial infarction in rats. *Eur J Pharmacol, 419*(2-3), 243-248.

Liao, J., Li, H., et al. (2012). Structural insight into the ion-exchange mechanism of the sodium/calcium exchanger. *Science, 335*(6069), 686-690. doi:10.1126/science.1215759

Ma, J., Guo, L., et al. (2011). High purity human-induced pluripotent stem cell-derived cardiomyocytes: electrophysiological properties of action potentials and ionic currents. *Am J Physiol Heart Circ Physiol, 301*(5), H2006-2017. doi:10.1152/ajpheart.00694.2011

Matsuda, T., Arakawa, N., et al. (2001). SEA0400, a novel and selective inhibitor of the Na+-Ca2+ exchanger, attenuates reperfusion injury in the in vitro and in vivo cerebral ischemic models. *J Pharmacol Exp Ther, 298*(1), 249-256.

Milani-Nejad, N., Janssen, P. M. (2014). Small and large animal models in cardiac contraction research: advantages and disadvantages. *Pharmacol Ther, 141*(3), 235-249. doi:10.1016/j.pharmthera.2013.10.007

Nicholas, S. B., Yang, W., et al. (1998). Alternative promoters and cardiac muscle cell-specific expression of the Na+/Ca2+ exchanger gene. *Am J Physiol, 274*(1), H217-232. doi:10.1152/ajpheart.1998.274.1.H217

OPTN. (2019, 10.01.2019). Organ Procurement and Transplantation Network Policy. Retrieved from https://optn.transplant.hrsa.gov/media/1200/optn_policies.pdf

Oravecz, K., Kormos, A., et al. (2018). Inotropic effect of NCX inhibition depends on the relative activity of the reverse NCX assessed by a novel inhibitor ORM-10962 on canine ventricular myocytes. *Eur J Pharmacol, 818*, 278-286. doi:10.1016/j.ejphar.2017.10.039

Otsomaa, L., Koskelainen, T., et al. (2004). Finland Patent No. WO2004063191A1. F. Orion Corporation.

Page, G., Ratchada, P., et al. (2016). Human ex-vivo action potential model for pro-arrhythmia risk assessment. *J Pharmacol Toxicol Methods, 81*, 183-195. doi:10.1016/j.vascn.2016.05.016

Parry, P. R., Bryce, M. R., et al. (2003). 5-Formyl-2-furylboronic acid as a versatile bifunctional reagent for the synthesis of pi-extended heteroarylfuran systems. *Org Biomol Chem, 1*(9), 1447-1449.

Primessnig, U., Bracic, T., et al. (2019). Long-term effects of Na+/Ca2+ exchanger inhibition with ORM 11035 improves cardiac function and remodeling without lowering blood pressure in a model of heart failure with preserved ejection fraction. *Eur J Heart Fail*.

Qu, Y., Page, G., et al. (2017). Action Potential Recording and Pro-arrhythmia Risk Analysis in Human Ventricular Trabeculae. *Front Physiol, 8*, 1109. doi:10.3389/fphys.2017.01109

Redfern, W. S., Carlsson, L., et al. (2003). Relationships between preclinical cardiac electrophysiology, clinical QT interval prolongation and torsade de pointes for a broad range of drugs: evidence for a provisional safety margin in drug development. *Cardiovasc Res, 58*(1), 32-45.

Ruch, S. R., Nishio, M., et al. (2003). Effect of cardiac glycosides on action potential characteristics and contractility in cat ventricular myocytes: role of calcium overload. *J Pharmacol Exp Ther, 307*(1), 419-428. doi:10.1124/jpet.103.049189

Selye, H., Bajusz, E., et al. (1960). Simple techniques for the surgical occlusion of coronary vessels in the rat. *Angiology, 11*, 398-407. doi:10.1177/000331976001100505

Shattock, M. J., Ottolia, M., et al. (2015). Na+/Ca2+ exchange and Na+/K+-ATPase in the heart. *J Physiol, 593*(6), 1361-1382. doi:10.1113/jphysiol.2014.282319

Sher, E., Gotti, C., et al. (1988). Intracellular calcium homeostasis in a human neuroblastoma cell line: modulation by depolarization, cholinergic receptors, and alpha-latrotoxin. *J Neurochem, 50*(6), 1708-1713.

Shpak, C., Hiller, R., et al. (2003). The endogenous inhibitor of NCX1 does not resemble the properties of digitalis compound. *Biochem Biophys Res Commun, 308*(1), 114-119.

Szentandrassy, N., Birinyi, P., et al. (2008). SEA0400 fails to alter the magnitude of intracellular Ca2+ transients and contractions in Langendorff-perfused guinea pig heart. *Naunyn Schmiedebergs Arch Pharmacol, 378*(1), 65-71. doi:10.1007/s00210-008-0296-5

Tanaka, H., Shimada, H., et al. (2007). Involvement of the Na+/Ca2+ exchanger in ouabain-induced inotropy and arrhythmogenesis in guinea-pig myocardium as revealed by SEA0400. *J Pharmacol Sci, 103*(2), 241-246.

Yatabe, M. S., Yatabe, J., et al. (2015). Effects of renal Na+/Ca2+ exchanger 1 inhibitor (SEA0400) treatment on electrolytes, renal function and hemodynamics in rats. *Clin Exp Nephrol, 19*(4), 585-590. doi:10.1007/s10157-014-1053-3

Ye, X. Y., Chen, S., et al. (2010). Synthesis and structure-activity relationships of 2-aryl-4-oxazolylmethoxy benzylglycines and 2-aryl-4-thiazolylmethoxy benzylglycines as novel, potent PPARalpha selective activators- PPARalpha and PPARgamma selectivity modulation. *Bioorg Med Chem Lett, 20*(9), 2933-2937. doi:10.1016/j.bmcl.2010.03.019

Zhang, J. (2013). New insights into the contribution of arterial NCX to the regulation of myogenic tone and blood pressure. *Adv Exp Med Biol, 961*, 329-343. doi:10.1007/978-1-4614-4756-6_28

Zhang, J., Ren, C., et al. (2010). Knockout of Na+/Ca2+ exchanger in smooth muscle attenuates vasoconstriction and L-type Ca2+ channel current and lowers blood pressure. *Am J Physiol Heart Circ Physiol, 298*(5), H1472-1483. doi:10.1152/ajpheart.00964.2009

Zornoff, L. A., Paiva, S. A., et al. (2009). Experimental myocardium infarction in rats: analysis of the model. *Arq Bras Cardiol, 93*(4), 434-440, 426-432.

Authors' contributions

L.O. had the main responsibility of devising the conceptualising the research project. J.L., N.J., L.V., A.V., E.M., and J.Gy.P. were responsible for pharmacological conceptualization. L.O., J.L., G.W., H.C., A.K., K.S., T.K., S.E.P.,P.F., A.H., and Z.K. performed the research and analysed the data. N.A.G., A.G., P.E.M., and G.P. were responsible for designing human tissue studies. L.O. and J. L. had the principal responsibility of writing and drafting the manuscript. N.A.G., E.M., and N.J critically reviewed the original draft of the manuscript and contributed to the writing process. G.W. critically commented on the manuscript.

Table 1. NCX inhibition values (n=3) and the selectivity profile towards hERG (n=4) and L-type Ca^{2+} channels (n=4) for selected example compounds. The abbreviation n refers to the number of independent plates.

Code	NCX IC_{50} nM	hERG IC_{50} µM	L-type Ca^{2+} IC_{50} µM	Solubility class
ORM-120407	231	2.1	3.1	insoluble
ORM-11023	156	-	-	-
ORM-11024	875	-	-	-
ORM-11165	4	9	2	insoluble
ORM-11217	210	14.6	-	moderate
ORM-11190	204	-	-	-
ORM-11298	31	>10	-	moderate
ORM-11372	6	10.6	6.1	moderate
ORM-11817	3	2.4	10.4	insoluble
ORM-11863	2.5	-	-	insoluble
ORM-11875	90	-	-	moderate

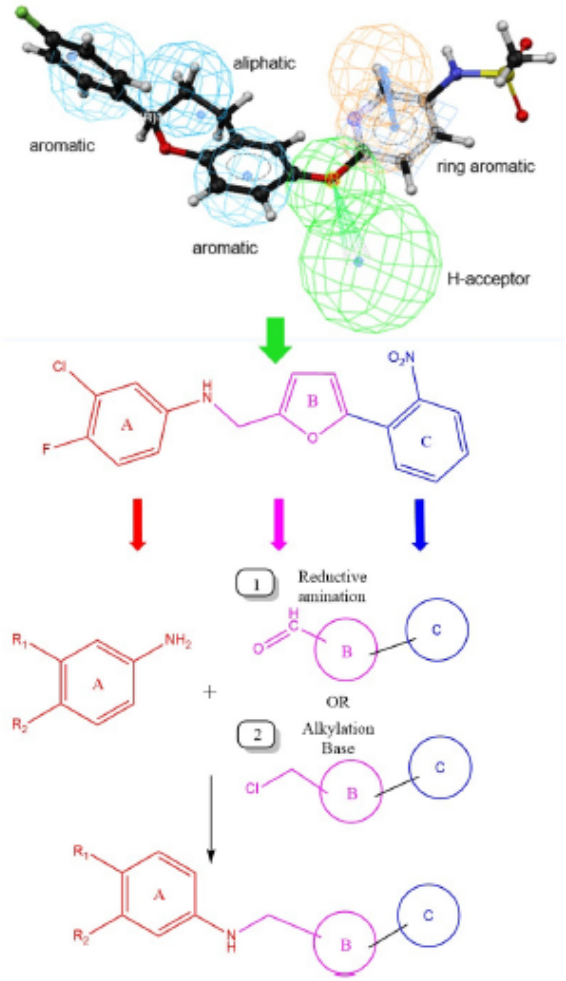

Figure 1. The upper part of the figure shows the pharmacophore model used for virtual screening. In-silico hits were further filtered based on predicted activity, clogS, clogP, and diversity. The middle part displays the hit structure and substructure features optimized in parallel processes. At the bottom of the figure, two routes used for the synthesis of the compounds are presented, namely reductive amination (1) and alkylation under basic conditions (2).

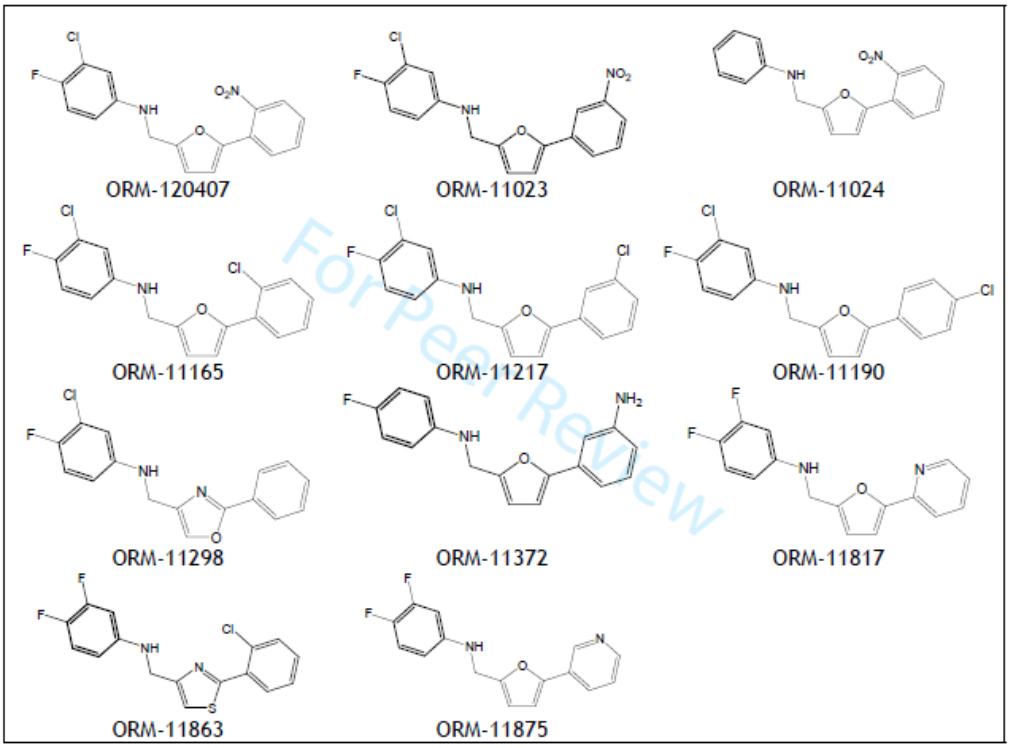

Figure 2. Illustrative chemical structures (out of 135 synthesized molecules) during the chemical optimization of the scaffold. ORM-11372 had the most favourable profile overall, out of the synthesized derivatives.

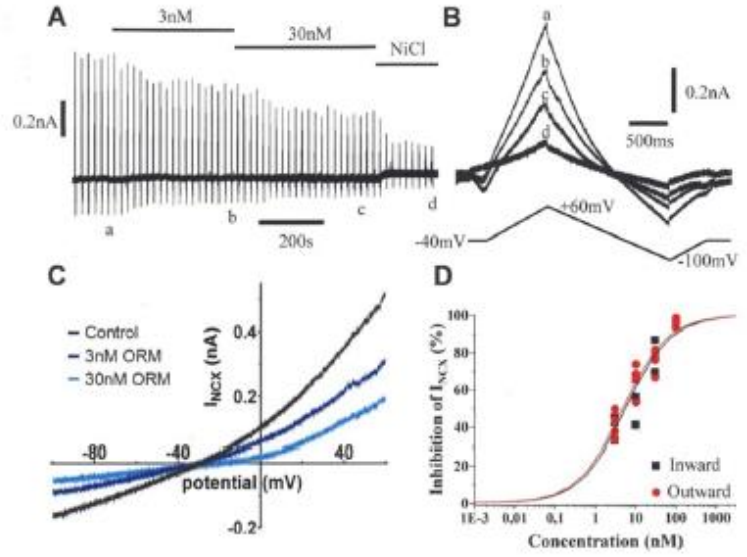

Figure 3. Effect of ORM-11372 on the bidirectional I_{NCX} of human iPS derived cardiomyocytes. (A) The experimental timecourse included a ramp voltage protocol to be repeated every 20 s. The current traces at the labels (a: control, b and c: in the presence of 3 and 30 nM ORM-11372, and d: when I_{NCX} is fully blocked by 10 mM $NiCl_2$ are shown in B enlarged and superimposed (with the voltage protocol below) images. (C) The concentration-response curve for ORM-11372 on the outward (3 nM n=4; 10 nM n=6; 30 nm n= 4; 100 nM n=3) and inward (3 nM n=4; 10 nM n=4; 30 nm n= 3; 100 nM n=2) I_{NCX} was determined at +60 and -100 mV, respectively. The IC_{50} values are calculated using nonlinear regression. Individual values are shown in the figure. The abbreviation n refers to number of iPS derived cardiomyocytes.

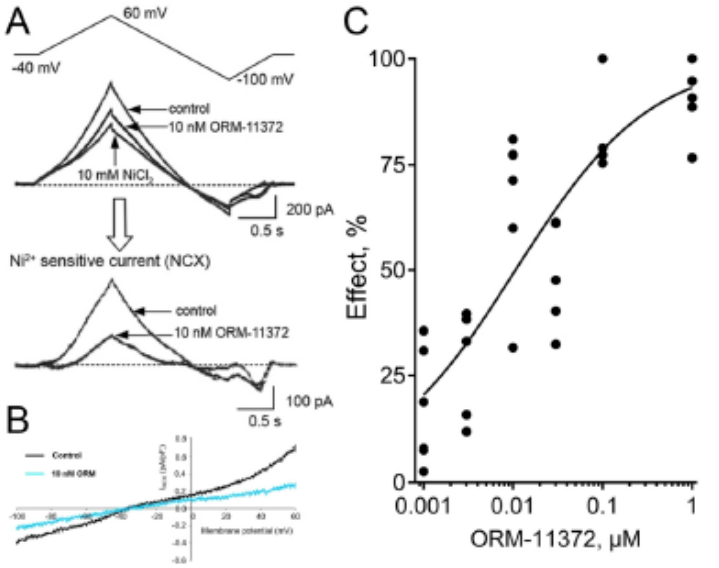

Figure 4. The effect of ORM-11372 on the reverse NCX current measured in rat ventricular cardiomyocytes is presented in the panel A. The top left panel A shows the voltage protocol applied during experiments: The I-V (current-voltage) relationship of the Na^+/Ca^{2+} exchanger current was measured through the use of ramp pulses at 20 s intervals. The ramp pulse initially lead to depolarization from the holding potential of -40 mV to 60 mV, at a rate of 100 mV/s, followed by hyperpolarization to -100 mV, and depolarization back to the holding potential. The middle panel illustrates original current records in the absence (control) and presence of 10 nM ORM-11372, and after applying 10 mM $NiCl_2$. The Ni^{2+} sensitive current traces clearly show that 10 nM ORM-11372 effectively inhibits the reverse NCX current. Example of the I-V (current-voltage) relationship of the Na^+/Ca^{2+} exchanger current is shown in the panel B. The magnitude of reverse NCX current measured at 20 mV was reduced by ORM-11372 in a concentration-dependent manner in rat ventricular cardiomyocytes in panel BC. The concentration-response curve for ORM-11372 on the outward (n = 5) and inward (n = 3) I_{NCX} was determined at +60 and -100 mV respectively. The IC_{50} value for the outward I_{NCX} current is calculated using nonlinear regression. Individual values are shown in the figure. The abbreviation n refers to number of rat primary ventricular cardiomyocytes.

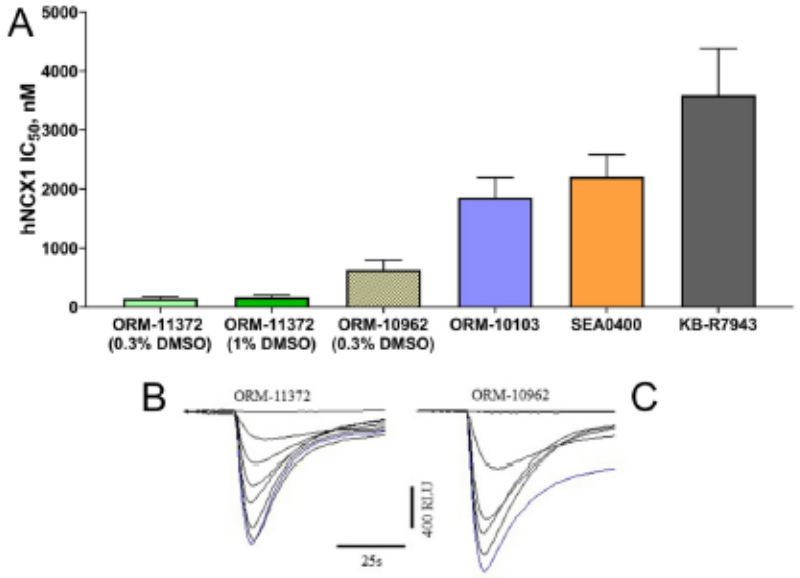

Figure 5. The effect of selected NCX inhibitors (n=5) were tested on the forward mode in confirmatory hNCX1 inhibition assay in HEK293 cells (A). Increasing concentrations of (B) ORM-11372 (0.001, 0.003, 0.01, 0.03, 0.1, 0.3 and 1μM) and (C) ORM-10962 (0.03, 0.1, 0.3, 1, 3 and 10μM) decreased Ca^{2+} efflux (downward deflection) from control conditions (blue trace). The abbreviation n refers to the number of plates (4 replicates per plate).

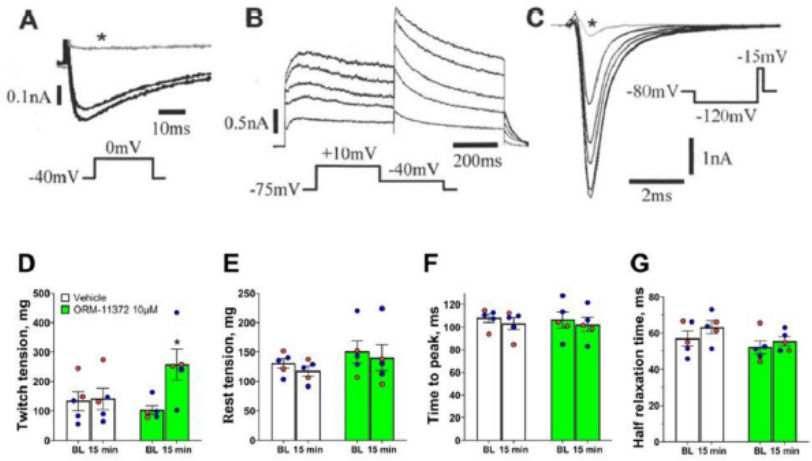

Figure 6. Effects of ORM-11372 on various cardiac ion channel currents of iPS derived cardiomyocytes (illustrative figures in panels A-C) and contraction force in guinea-pig papillary muscle (panels D-G). (A) The L-type I_{Ca} was minimally inhibited by 1 μM ORM-11372. (B) The concentration-dependent inhibition of $K_V11.1$ current by 0.3, 3, 10, and 30 μM ORM-11372 and (C) $Na_V1.5$ current by 1, 3, 10, and 30 μM ORM-11372. The applied voltage protocols are shown as insets. The traces marked by asterisk in A and C are the currents in the presence of 100 nM nitrendipine and 2 mM lidocaine, respectively. (D) ORM-11372 increased twitch tension which indicates increased SR load. (E) ORM-11372 did not increase rest tension i.e. no increase in diastolic calcium. (F) ORM-11372 did not affect time to peak which demonstrate that calcium release from ryanodine receptors is normal. (G) Also half relaxation time was unchanged showing that SERCA function remains normal. Shown are mean (± SEM, n=5) and individual values with red and blue circle for female and male, respectively. Two-way ANOVA followed by Sidak's multiple comparison test. *p<0.05. Pacing rate 1 Hz. Temperature 37 °C.

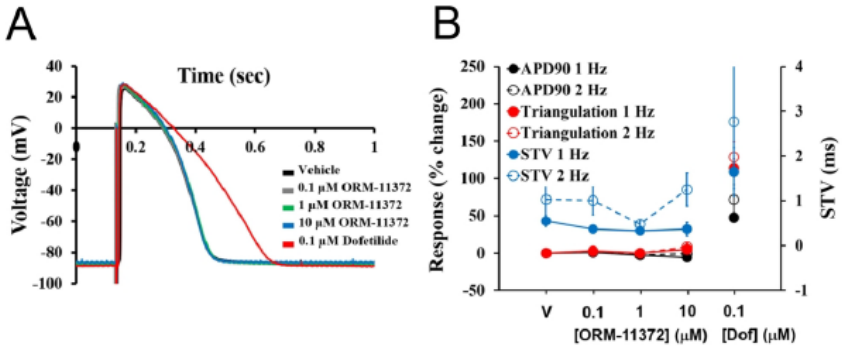

Figure 7. Effects of ORM-11372 on action potentials (APs) in human ventricular *trabeculae* (n = 2, 2 replicates). (A) Typical APs recorded from a human ventricular *trabecula* at a pacing rate of 1 Hz in the presence of vehicle control, and after exposure to ORM-11372 (0.1, 1 and 10 μM) and 0.1 μM dofetilide (the positive control). (B) Mean changes in APD_{90}, triangulation, and STV values were in cadence when *trabeculae* were incubated with ORM-11372 and dofetilide at 1 and 2 Hz. Notably, the effects of ORM-11372 and dofetilide on APD_{90}/triangulation activity and STV are plotted on a separate y-axis. V: Vehicle; Dof, Dofetilide; H: Heart; T: *Trabecula*. The abbreviation n refers to the number of human hearts and replicates refer to the number of *trabeculae* in the same heart.

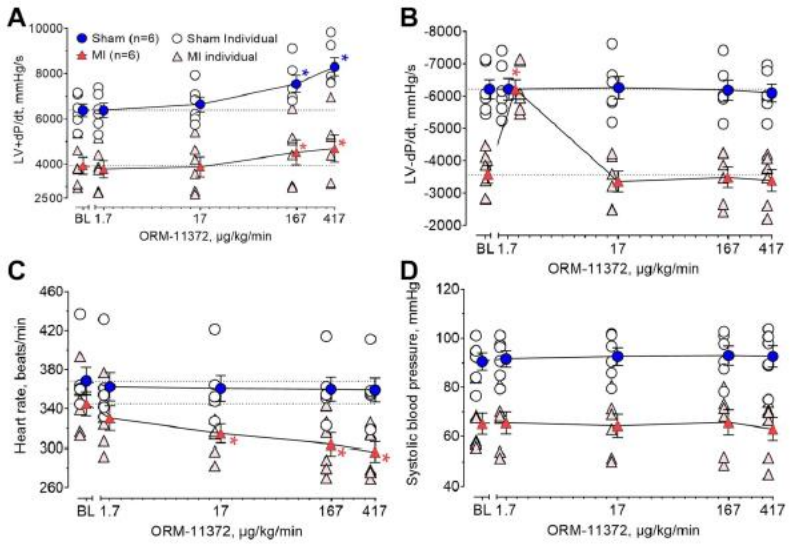

Figure 8. Effects of ORM-11372 on hemodynamics in isoflurane anesthetized rats, 7 days after the induction of myocardial infarction (MI n=6, SHAM n=6). Effects on the left ventricular contractility ($LV+dP/dt_{max}$) are shown in panel A, along with values for relaxation ($LV-dP/dt_{max}$, B), heart rate (C), and systolic arterial blood pressure (D). *p<0.05 A two-way repeated measures ANOVA was followed by the Dunnet's posthoc test. Values are shown as mean ± SEM. The abbreviation n refers to the number of rats.

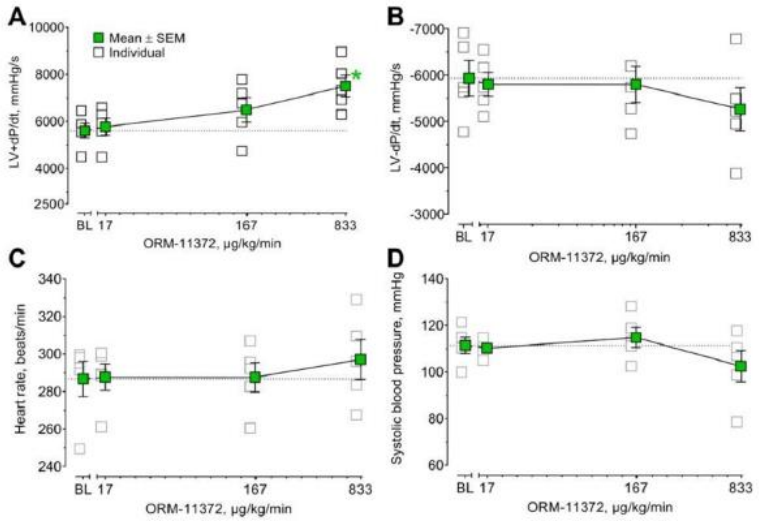

Figure 9. Effects of ORM-11372 on hemodynamics in S-ketamine anesthetized rabbits (n=5). In panel A, the effects on the left ventricular contractility ($LV+dP/dt_{max}$), relaxation ($LV-dP/dt_{max}$, B), heart rate (C), and systolic arterial blood pressure (D) are shown. *$p<0.05$. A one-way repeated measures ANOVA was followed by Dunnet's posthoc test. Values are shown in terms of mean ± SEM. The abbreviation n refers to the number of rabbits.